MDPI

Article

Nb and REE Distribution in the Monte Verde Carbonatite–Alkaline–Agpaitic Complex (Angola)

Sandra Amores-Casals [1,2,*], Antonio Olimpio Gonçalves [3], Joan-Carles Melgarejo [1]
and Joan Martí Molist [4]

1   Departament de Mineralogia, Petrologia i Geologia Aplicada, Universitat de Barcelona, 08028 Barcelona, Spain; joan.carles.melgarejo.draper@ub.edu
2   Geomar Enginyeria del Terreny SLP, 08015 Barcelona, Spain
3   Departamento de Geologia, Facultade de Ciências, Universidade Agostinho Neto, Luanda, Caixa Postal 815, Angola; tonygoncalves72@hotmail.com
4   Institut de Ciències de la Terra Jaume Almera, Consejo Superior de Investigaciones Científicas (CSIC), 08028 Barcelona, Spain; joan.marti@ictja.csic.es
*   Correspondence: sandra.amores.casals@gmail.com; Tel.: +34-625-099-009

check for updates

Abstract: The Angolan alkaline–carbonatite complex of Monte Verde has a semi-circular shape and is comprised of a central intrusion of foidolite rocks surrounded by concentrically arranged minor bodies of other alkaline rocks and carbonatite magmatic breccias. This rock association is hosted by fenitized Eburnean granites. Concentric swarms of alkaline dykes of late formation, mostly of nepheline trachyte composition, crosscut the previous units. Most high-field strength elements (HFSE) and rare earth elements (REE) are concentrated in pyrochlore crystals in the carbonatite and alkaline breccias. Magmatic fluornatropyrochlore is replaced and overgrown by five secondary generations of pyrochlore formed during subsolidus stages and have higher Th, REE, Si, U, Sr, Ba, Zr, and Ti contents. The second, third, and fourth pyrochlore generations are associated with late fluids also producing quartz and REE rich minerals; whereas fifth and sixth pyrochlore generations are linked to the fenitization process. On the other hand, minerals of the rinkite, rosenbuschite, wöhlerite, eudialyte groups, as well as loparite-(Ce), occur in accessory amounts in nepheline trachyte, recording low to moderate agpaicity. In addition, minor REE-bearing carbonates, silicates, and phosphates crystallize as late minor secondary minerals into carbonatite breccia and alkaline dykes. In conclusion, the scarcity of HFSE and REE minerals at the Monte Verde carbonatite-alkaline-agpaitic complex suggests low metallogenetic interest and economic potential for the outcrops analysed in this study. However, the potential for buried resources should not be neglected.

Keywords: Nb; pyrochlore; carbonatite; magmatic breccia; alkaline subsaturated rocks; agpaitic minerals; eudialyte; rinkite; loparite; Angola

1. Introduction

Undersaturated alkaline rocks and their pegmatoid facies have been traditionally considered as one of the main resources for many rare elements (e.g., [1–8]).

Over the last year, research has been done on the latter as a potential source for critical elements, such as REE [9–16], Nb [17], and Be [18–21]. This has led to an increased interest in alkaline magmatic terrains due to their association with carbonatites enriched in critical elements (e.g., [8,22]).

The Monte Verde alkaline–carbonatite complex, located between Huambo and Kwanza Sul provinces, is one of the least studied carbonatite complexes in Angola. As a few studies have reported, the Monte Verde complex is comprised of nepheline syenites and several carbonatite bodies cropping out in an arcuate area of fenitized granitic host-rocks. Magmatic breccias are set into the alkaline rocks,

which, in turn, are cut by late dykes of alkaline affinity [8,23,24]. Nevertheless, the structure of Monte Verde is poorly constrained, and mineralogical and textural studies have never been carried out.

Recently, significant rare element concentrations have been found in other Angolan carbonatites of the Lucapa structure, such as Tchivira [25,26], Bonga [26–30], Virulundo [31], Bailundo [32], and Catanda [33]. Therefore, an accurate examination of Monte Verde is required as it could also hold significant metallogenetic potential. Furthermore, despite the fact that breccia occurrence can provide key information about rare element distribution during explosive events, this process is not yet well understood. Thus, we present the study of the Monte Verde carbonatitic complex in order to provide a comprehensive approach on its metallogenetic potential. First, we defined and mapped the carbonatite and alkaline units. Then, we conducted a detailed petrographic characterization and mineral chemistry analysis of HFSE- and REE-bearing minerals—mainly pyrochlore, REE in carbonates and phosphates, as well as Na-Ti-Nb-Zr-REE in sorosilicates and oxides of the carbonatite and alkaline rocks—as a guide to understanding the distribution of rare elements. Finally, we discuss the metallogenetic potential of the Monte Verde complex.

2. Geological Setting

The Monte Verde complex is located between Kwanza Sul, Benguela, and Huambo provinces, 500 km from the capital of Angola, Luanda (Figure 1). Monte Verde is related to the Lucapa graben, an extensional rift structure cutting the Congo, Kasai, and Angola Cratons since the opening of the South Atlantic Ocean began and after the Early Cretaceous [34,35]. Kimberlite and carbonatite rocks are associated with this rifting process. Most Angolan kimberlites outcrop at the north-eastern provinces; however, carbonatite complexes occur in central and south-western areas, usually related to alkaline rocks [8]. Dating of alkaline intrusions at the Lucapa graben has demonstrated that all of them were emplaced during the Early Cretaceous [29,36–38]. However, geochronological studies of the carbonatite lavas in Catanda (Kwanza Sul province) show ages of 0.5 Ma [33,39]; thus, suggesting Quaternary extensional activity at the Lucapa graben.
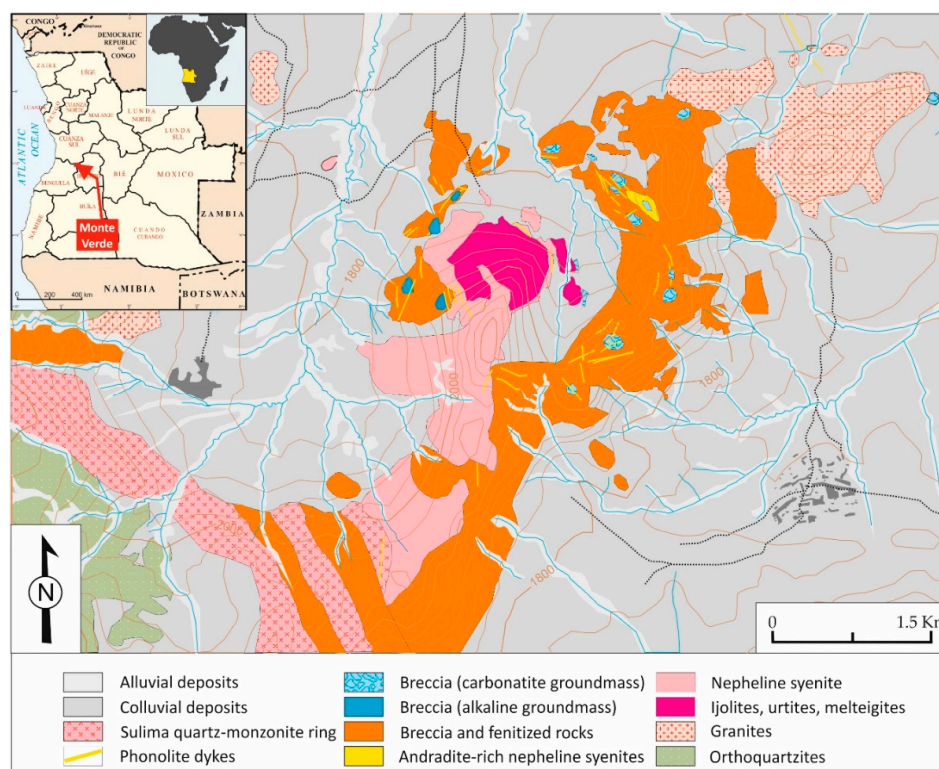
Figure 1. Geological map of Monte Verde complex obtained by joining our data with those of [23]. Path and roads are marked as dotted lines. The Angolan town of Cambambe is located on the left side of the map.

3. Materials and Methods

Sampling and mapping of the Monte Verde complex were done in a 2014 field campaign. A total of 95 samples of plutonic alkaline rocks, alkaline dykes, breccia, and fenitized granites were selected and collected. About 76 polished thin sections were prepared and studied in order to identify mineral phases and textural features using transmitted and reflected optical microscopy with plane polarized light. The most representative regions were selected for further analysis by SEM-EDS.

A total of 21 selected samples were studied in detail with SEM-BSE-EDS. Qualitative analyses and detailed characterization of mineral textures were done using a Quanta ESEM Quanta Q-200 FEI XTE 325/D8395 Scanning Electron Microscope (Thermo Fisher Scientific, Waltham, MA, USA) coupled with an INCA Energy 250 EDS microanalysis system, located at the Scientific and Technological Centres of the University of Barcelona. Operating conditions were 20 keV, 1 nA beam current, and 10 mm working distance.

Seven samples were selected in order to quantify Nb and REE bearing phases using a JEOL JXA-8230 electron microprobe (JEOL USA, Peabody, MA, USA) with five wavelength dispersive spectrometers (JEOL USA, Peabody, MA, USA), also located at the Scientific and Technological Centres of the University of Barcelona. Operating conditions used were the following: pyrochlore, 20 kV and 14.4 nA; Na-Ti-Zr-REE silicates, 20 kV and 14.7 nA; perovskite and loparite, 20 kV and 14.9 nA; REE carbonates and phosphates, 20 kV and 6.5 nA. For all elements, the counting time was 10 s peak and 10 s background except for Ce, La, Ba (20 s peak and 20 s background), and Na and F (30 s peak and 30 s background). The acquisition method used was two background measurements at each side of the peak. The beam diameter was 5 μm. Standards and lines used are listed in Table 1. A total of 681 analyses were obtained.

Table 1. Standards, X-ray, and crystal used.

Pyrochlore and Perovskite-loparite (Element, Standard, X-ray and Crystal)	Na-Ti-Zr Silicates (Element, Standard, X-ray and Crystal)	REE Carbonates and REE Phosphates (Element, Standard, X-ray and Crystal)
U (UO_2, Mβ, PETJ)	Si (Wollastonite, Kα, TAP)	Si (Wollastonite, Kα, TAP)
K (Orthoclase, Kα, PETJ)	Al (Corundum, Kα, TAP)	Ce (CeO_2, Lα, PETJ)
Th (ThO_2, Ma, PETJ)	Hf (Hf, Mα, TAP)	La (LaB_6, Lα, PETJ)
Ti (Rutile Kα, PETJ)	Ti (Rutile Kα, PETJ)	Ba (Barite, Lα, LIFH)
La (LaB_6, Lα, PETJ)	La (LaB_6, Lα, PETJ)	F (Apatite, Kα, TAPH)
Ce (CeO_2, Lα, PETJ)	Ce (CeO_2, Lα, PETJ)	Gd ($Gd_3Ga_5O_{12}$, Lβ, LIFH)
Al (Corundum, Kα, TAPH)	Mg (Periclase, Kα, TAPH)	Fe (Fe_2O_3, Kα, LIFH)
Mg (Periclase, Kα, TAPH)	Na (Albite, Kα, TAPH)	Sm (REE^{-3}, Lβ, LIFH)
Na (Albite, Kα, TAPH)	F (Apatite, Kα, TAPH)	Mn (Rhodonite, Kα, LIFH)
Si (Wollastonite, Kα, TAPH)	Ta (Ta, Lα, LIFH)	Nd (REE^{-4}, Lβ, LIFH)
F (Fluorite, Kα, TAPH)	Fe (Fe_2O_3, Kα, LIFH)	Pr (REE^{-1}, Lβ, LIFH)
Ba (Barite, Lα, LIFH)	Mn (Rhodonite, Kα, LIFH)	Ca ($CaCO_3$, Kα, PETL)
Nd (REE^{-4}, Lβ, LIFH)	Ba (Barite, Lα, LIFH)	U (UO_2, Mβ, PETJ)
Mn (Rhodonite, Kα, LIFH)	Ca (Wollastonite, Kα, PETL)	Th (ThO_2, Ma, PETJ)
Sm (REE^{-3}, Lβ, LIFH)	K (Orthoclase, Kα, PETJ)	P (Apatite, Kα, TAPH)
Fe (Fe_2O_3, Kα, LIFH)	Cl (AgCl, Kα, PETL),	Y (YAG, Lα, PETL)
Ta (Ta, Lα, LIFH)	Nb (Nb, Lα, PETL)	Sr (Celestine, Lα, PETL)
Ca (Wollastonite, Kα, PETL)	Zr (ZrO_2, Lα, PETL)	
Pb (PbS, Mα, PETL)	Sr (Celestine, Lα, PETL)	
Nb (Nb, Lα, PETL)		
Zr (ZrO_2, Lα, PETL)		
Sr (Celestine, Lα, PETL)		

4. Results

4.1. Monte Verde Carbonatite Structure

The Monte Verde complex displays a concentric semi-circular structure defined by alkaline rocks surrounded by fenitized Precambrian granites. Colluvial and alluvial deposits cover the central and north-western area, hiding most outcrops. No intrusive carbonatite bodies occur, and only a few small outcrops of carbonatite breccia have been distinguished. However, carbonatitic rocks are very common in most of the other sub-volcanic Angolan complexes, such as Tchivira, Bonga, Virulundo, or Bailundo [26,27,31,32].

The complex presents a central unit comprised of two plutonic alkaline rock types, according to their nepheline and feldspar contents (Figure 1). Nepheline syenites are made up of K-feldspar and lesser nepheline (Figure 2a), whereas andradite-rich nepheline syenites in the north-eastern zone have high andradite-schorlomite contents. In addition, three different foidolites (urtites, ijolites, and melteigites) appear at the centre of the complex in contact with the nepheline syenites, with higher contents of feldspathoids, such as nepheline, sodalite, or cancrinite, and an absence of feldspar (Table 2).
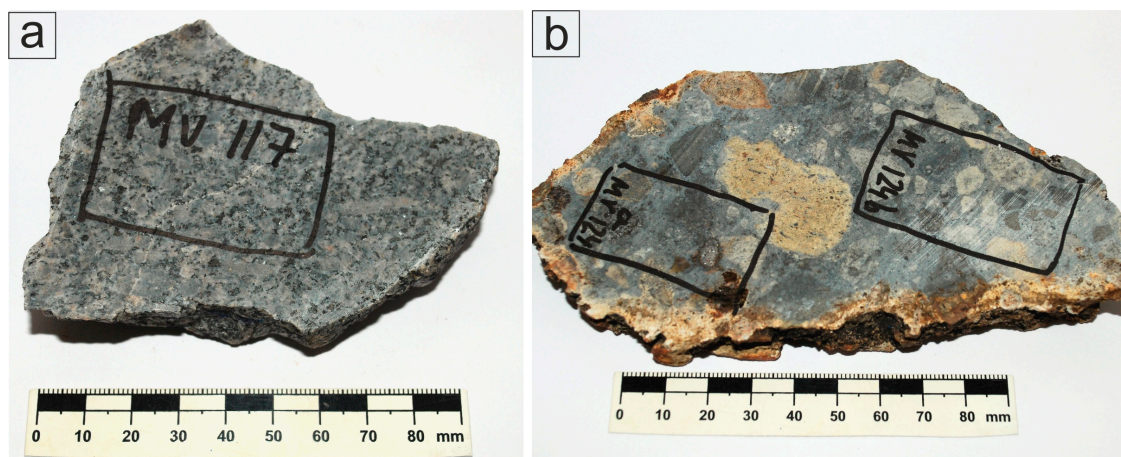
Figure 2. (**a**) Nepheline syenite from the Monte Verde central intrusion. (**b**) Magmatic breccia with an alkaline groundmass with fragments of calciocarbonatite and fenitized granites.

An external aureole of fenitization surrounds these plutonic rocks (Figure 1). Fenitization processes have extensively replaced the granites (Figure 1), and the alteration is more intensive near the carbonatite and plutonic alkaline rocks. Dominant K-feldspar stained by hematite gives a rose-reddish tone to these rocks, which strongly differentiates them from the unaltered Precambrian host rock.

Magmatic breccia outcrops occur among fenitized granites. Carbonatite and alkaline breccias can be distinguished according to the composition of the groundmass. Carbonatite breccias mainly contain fenitized granite xenoliths of variable size, ranging from microscopic to metric dimensions with an angular shape, suggesting an absence of assimilation by the carbonatite mesostase. The mesostase corresponds to a calciocarbonatite, as calcite is the major phase with lesser apatite, pyrite, and pyrochlore (Table 2).

Alkaline breccia (Figure 2b) outcrops are scarce and located among fenitized rocks surrounding the central alkaline intrusion. Two main types of alkaline breccias can be distinguished based on the ratio of host rock fragments with respect to the mesostase. In one case, the proportion of fragments is dominant over that of the mesostase, and in another, the opposite is true. Both breccia may concentrate Nb and REE minerals.

Four types of alkaline dykes of metric to decametric width cut all the above-mentioned rocks (Figure 1). Sodalite trachyte, nepheline trachyte, tinguaite, and latite dykes present porphyry textures with K-feldspar, augite, and nepheline as phenocrysts. Trace amounts of Na-Ti-Ce-Zr sorosilicates of the eudialyte and rinkite groups, REE-bearing oxides, such as those of the perovskite-loparite series, and REE carbonates and phosphates occur as disseminations in the rock.

Table 2. Minerals forming the main units of the Monte Verde Complex.

Group	Mineral	Formula	Unit
		Tectosilicates	
Quartz	Quartz	SiO_2	Fenites; matrix-supported alkaline breccia
Feldspar group	K-feldspar Albite	$KAlSi_3O_8$ $NaAlSi_3O_8$	Andradite-bearing nepheline syenite; fenites; matrix-supported alkaline breccia; alkaline dykes
Feldspathoid group	Nepheline-kalsilite	$(Na,K)AlSiO_4$	Foidolites; andradite-bearing nepheline syenite; fenites; matrix-supported alkaline breccia; alkaline dykes
	Sodalite	$Na_8(Al_6Si_6O_{24})Cl_2$	Foidolites; andradite-bearing nepheline syenite; fenites; matrix-supported alkaline breccia; alkaline dykes
	Cancrinite	$(Na,Ca,\square)_8(Al_6Si_6O_{24})(CO_3,SO_4)_2 \cdot 2H_2O$	Foidolites; andradite-bearing nepheline syenite; matrix-supported alkaline breccia; alkaline dykes
		Phyllosilicates	
Mica group	Phlogopite-tetraferriphlogopite	$KMg_3(Fe^{3+}Si_3O_{10})(OH,F)_2$	Foidolites
	Phlogopite-annite	$K(Mg,Fe^{2+})_3(AlSi_3O_{10})(OH)_2$	Foidolites; fenites; matrix-supported alkaline breccia
		Inosilicates	
Clinopyroxene group	Aegirine augite	$(Ca,Na(Mg,Fe^{2+}Fe^{3+})(Si_2O_6)$	Foidolites; andradite-bearing nepheline syenite; fenites; breccia carbonatite groundmass; alkaline dykes
	Diopside	$CaMgSi_2O_6$	Foidolites (ijolites)
Amphibole group	Kaersutite	$NaCa_2\{Mg_3AlTi\}(Al_2Si_6O_{22})O_2$	Foidolites
	Arfvedsonite	$NaNa_2(Fe^{2+}_4Fe^{3+})Si_8O_{22}(OH)_2$	Foidolites
	Richterite–ferrorichterite	$Na(NaCa)(Mg,Fe^{2+})_5Si_8O_{22}(OH)_2$	Fenites; calciocarbonatite fragments; matrix-supported alkaline breccia
		Cyclosilicates	
Eudialyte group	Eudialyte	$Na_{15}Ca_6(Fe^{2+},Mn^{2+})_3Zr_3[Si_{25}O_{73}](O,OH,H_2O)_3(OH,Cl)_2$	Alkaline dykes
		Sorosilicates	
Rinkite group	Rosenbuschite	$Na_6Ca_6Zr_3Ti(Si_2O_7)_4O_2F_6$	Melteigite; alkaline dykes
	Mosandrite-(Ce)	$(Ca_3REE)[(H_2O)_2Ca_{0.5}\square_{0.5}]Ti(Si_2O_7)_2(OH)_2(H_2O)_2$	Alkaline dykes
	Rinkite	$(Ca_3Ce)Na(NaCa)Ti(Si_2O_7)_2(OF)F_2$	Melteigite; alkaline dykes
Wöhlerite group	Wöhlerite	$NaCa_2(Zr,Nb)(Si_2O_7)(O,OH,F)_2$	Andradite-bearing nepheline syenite; alkaline dykes
		Nesosilicates	
Titanite group	Titanite	$CaTi(SiO_4)O$	Foidolites (urtites, melteigites); alkaline dykes
Garnet group	Andradite-schorlomite	$Ca_3Fe^{3+}_2(SiO_4)_3-Ca_3(Ti,Fe^{3+})_2((Si,Fe^{3+})O_4)_3$	Foidolites (ijolites); andradite-bearing nepheline syenite
Zircon group	Zircon	$Zr(SiO_4)$	Andradite-bearing nepheline syenite; matrix-supported alkaline breccia
Britholite group	Britholite-(La),	$Ca_2(La,Ce,Ca)_3(SiO_4,PO_4)_3(OH,F)$	Foidolites (melteigite)
	Britholite-(Ce)	$(Ce,Ca)_5(SiO_4)_3OH$	Alkaline dykes

Table 2. *Cont.*

Group	Mineral	Formula	Unit
		Oxides	
Ilmenite group	Ilmenite	$Fe^{2+}TiO_3$	Matrix supported alkaline breccia; alkaline dykes
Oxyspinel group	Ulvöspinel	$TiFe_2O_4$	Foidolites; alkaline dykes
Rutile group	Rutile	TiO_2	Fenites; calciocarbonatite fragments
	Ilmenorutile	$Fe_x(Nb,Ta)_{2x} \cdot 4Ti_{1-x}O_2$	Matrix supported alkaline breccia
Diaspore group	Goethite	α-$Fe^{3+}O(OH)$	Fenites
Hematite group	Hematite	Fe_2O_3	Matrix supported alkaline breccia
Pyrochlore group	Fluornatro-pyrochlore	$(Na,Ca)_2Nb_2O_6F$	Calciocarbonatite fragments; matrix-supported alkaline breccia
	Secondary Pyrochlore (II, III, IV, V, VI)	$(\square,Ca,Th,U,Ba,Sr,REE)_2\ Nb_2O_6(OH,F)$	Andradite-bearing nepheline syenite; calciocarbonatite fragments; matrix-supported alkaline breccia; breccia with carbonatite groundmass; alkaline dykes
Perovskite group	Perovskite	$CaTiO_3$	Alkaline dykes
	Loparite-(Ce)	$(Na,REE)Ti_2O_6$	Alkaline dykes
		Sulphides	
Pyrite group	Pyrite	FeS_2	Fenites; calciocarbonatite fragments; alkaline dykes
Galena group	Galena	PbS	Fenites; matrix-supported alkaline breccia
Sphalerite group	Sphalerite	ZnS	Matrix supported alkaline breccia
Pyrrhotite group	Pyrrhotite	Fe_7S_8	Foidolites (urtites melteigite); matrix-supported breccia
Pentlandite group	Pentlandite	$(Fe_xNi_y)_{\Sigma 9}S_8$	Foidolites (urtites melteigite)
		Sulphates	
Baryte	Baryte	$BaSO_4$	Fenites; calciocarbonatite fragments; matrix-supported breccia
		Phosphates	
Apatite group	Apatite	$Ca_5(PO_4)_3(Cl/F/OH)$	Calciocarbonatite fragments; matrix-supported breccia; breccia with carbonatite groundmass
Rhapdophane group	Rhabdophane-(Ce)	$Ce(PO_4) \cdot H_2O$	Fenites; alkaline dykes
		Halides	
Fluorite group	Fluorite	CaF_2	Calciocarbonatite fragments; matrix-supported breccia
		Carbonates	
Calcite group	Calcite	$CaCO_3$	Melteigite; andradite-bearing nepheline syenite; fenites; calciocarbonatite fragments; matrix-supported breccia; breccia with carbonatite groundmass; alkaline dykes
Dolomite group	Ankerite	$Ca(Fe^{2+},Mg)(CO_3)_2$	Fenites
Aragonite group	Strontianite	$SrCO_3$	Fenites; calciocarbonatite fragments
Synchysite group	Synchysite-(Ce)	$CaCe(CO_3)_2F$	Melteigite; calciocarbonatite fragments; matrix-supported breccia; alkaline dykes

Table 2. *Cont.*

Group	Mineral	Formula	Unit
Ancylite group	Ancylite-(Ce)Calcioancylite-(Ce)	$CeSr(CO_3)_2(OH) \cdot H_2O$ $(Ce,Ca,Sr)CO_3(OH,H_2O)$	Fenites; calciocarbonatite fragments; matrix-supported breccia; alkaline dykes
Burbankite group	Burbankite	$(Na,Ca)_3(Sr,Ba,Ce)_3(CO_3)_5$	Calciocarbonatite fragments; matrix-supported breccia; breccia with carbonatite groundmass; alkaline dykes
-	Carbocernaite	$(Ca,Na)(Sr,Ce,Ba)(CO_3)_2$	Alkaline dykes
Bastnäsite group	Th-rich bastnäsite-(Ce)	$Ce(CO_3)F$	Fenites
-	Daqingshanite-(Ce)	$(Sr,Ca,Ba)_3(Ce,La)(CO_3)_{3-x}(PO_4)(OH,F)_{2x}$	Fenites

Pervasive quartz alteration with Fe-oxides fills late fractures in the south and south-eastern ring area occupied by the fenites. At central and north-western regions, alluvial and colluvial deposits form a thick cover with clay deposits and rock fragments from alkaline and fenitized units.

4.2. Petrography of the Monte Verde Units: Occurrence of Nb and REE Phases

4.2.1. Plutonic Alkaline Rocks

The central intrusion of Monte Verde is made up of foidolite. They present a phaneritic holocrystalline texture, often symplectitic, with major nepheline, mafic minerals, very minor sodalite, and no K-feldspar. Urtite, the most abundant rock type, contains major nepheline, up to 95 modal %. It contains kalsilite exsolutions and is partly replaced by small amounts of sodalite and altered to secondary cancrinite. Aegirine augite (partly overgrown by kaersutite rims and arfvedsonite), titanite, ulvöspinel, and pyrrhotite with pentlandite exsolutions are accessory minerals. At the same location, melteigites have the same texture and similar composition as urtites, with major nepheline but display an agpaitic texture and contain higher contents of aegirine augite, kaersutite, pyrrhotite, ulvöspinel, and, locally, phlogopite-tetraferriphlogopite.

Minor ijolite outcropping at the central intrusion show intermediate compositions between urtite and melteigite. Aegirine augite and diopside are the major phases intergrown with nepheline and lesser phlogopite-annite. These ijolites have accessory amounts of reddish to brownish garnets of the andradite-schorlomite solid solution. In addition, scarce subhedral rosenbuschite grains (up to 1 mm in length), overgrown by rinkite rims, replace titanite and augite (Figure 3a). Rare britholite-(La) anhedral crystals of a few hundred microns in length also occur replacing titanite grains. A late association of calcite and radial aggregates of synchysite crystals, less than 10 μm in length, replaces the ensemble.

At the northwestern sector, andradite-bearing nepheline syenites intrude fenitized granites (Figure 1). K-feldspar is the most abundant mineral and is intergrown with nepheline (the last, strongly replaced by fine cancrinite) and with minor aegirine augite. The accessory Ca-bearing garnet has a high andradite-schorlomite component and forms euhedral grains partly replaced by fine-grained zircon, calcite, and locally, a very fine intergrowth with an HFSE and REE mineral, probably corresponding to fergusonite-(Nd). In addition, an unknown primary silicate (probably eudialyte, up to 1 mm in diameter) is completely substituted by a complex fine-grained intergrowth of calcite, albite, zircon, pyrochlore, and wöhlerite (Figure 3b).

4.2.2. Fenitized Granites

Eburnean fenitized granites comprise the most extensive unit of the Monte Verde carbonatite complex, roughly forming a ring shape of hectometric width surrounding the central alkaline intrusion. Fenitization is intimately associated with hydrothermal fluids involved during carbonatite formation, leading to the formation of alkaline rocks mostly at the contact between carbonatite and host rock [40,41]. Fenitization intensity progressively decreases from the contact with the intrusions of carbonatitic or alkaline rocks, so distal granites may preserve primary compositions and textures. At Monte Verde, fenitization is mainly K-rich as K-feldspar and biotite are pervasive. However, Na alteration made up of albite, richterite, nepheline, and sodalite occurs overprinting the K-rich alteration. At the same time, Na alteration was replaced by quartz and calcite.

Fenitized granites from the outermost areas present remnants of primary plagioclase with late fine microcline rims indicative of incipient K-fenitization. At the easternmost ring, fenites also contain fine-grained aegirine augite, in addition to biotite and pyrite. These minerals can be veined and replaced by Mn-rich ankerite followed by a complex mineral sequence with REE, HFSE, and LILE, including strontianite, calcioancylite-(Ce), barite, galena, Th-rich bastnäsite-(Ce), fine-grained rutile (Figure 3c), Th- and Ce-rich pyrochlore, and daqingshanite-(Ce) (Figure 3d). Most of these minerals occur in anhedral crystals, less than 30 μm in diameter. Quartz and calcite late veins replace all these minerals. Weathering of micas produced mixtures of vermiculite and smectite, and pyrite is replaced by goethite.
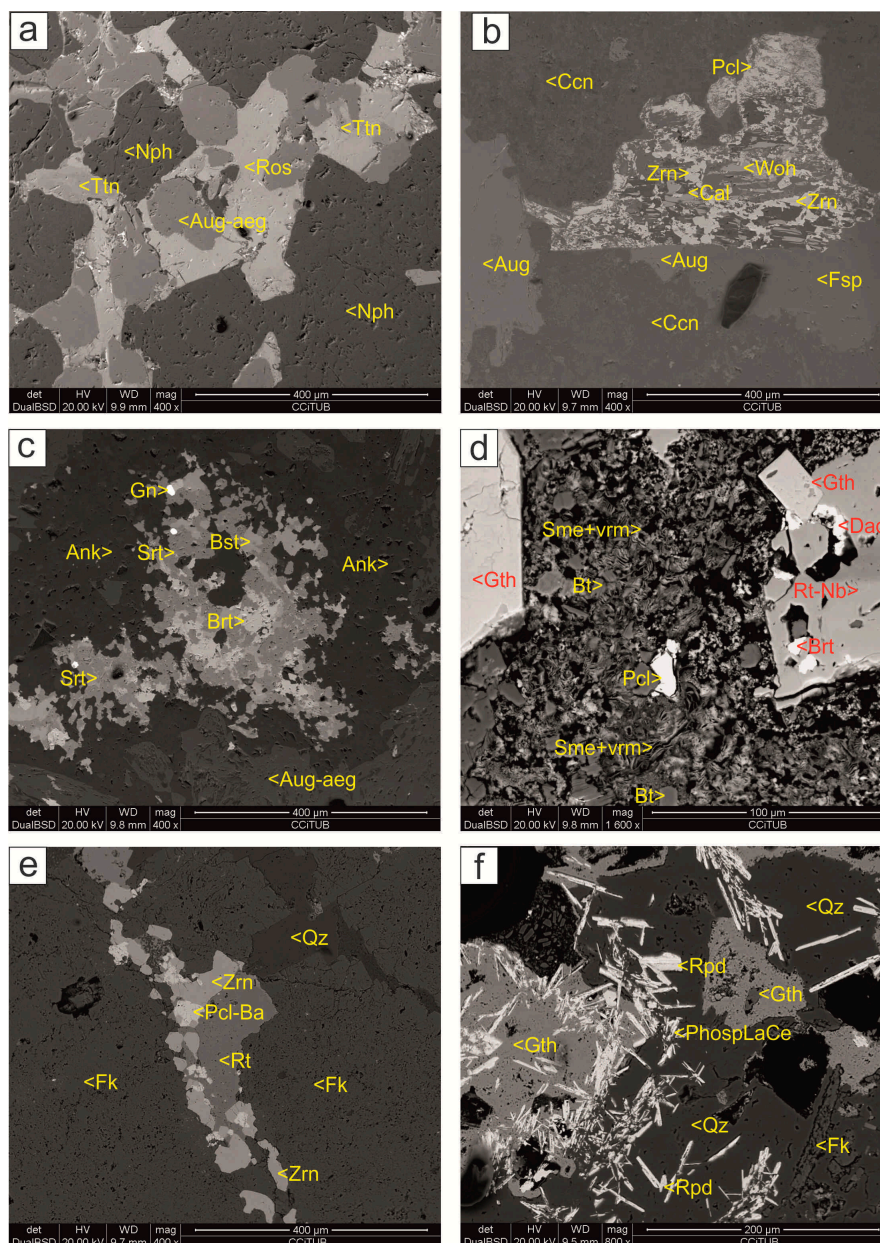
Figure 3. Nb and REE phases of the alkaline plutonic rocks and fenitized granites of Monte Verde; SEM images, BSE mode. (**a**) Melteigite with rosenbuschite (Ros) replacing aegirine augite (Aug-aeg), titanite (Ttn), and nepheline (Nph). (**b**) Detail of an andradite-bearing nepheline syenite with K-feldspar (Fsp), nepheline pseudomorphs after cancrinite (Ccn), augite (Aug), and an unknown primary phase (probably eudialyte) totally replaced by a mixed association of calcite (Cal), albite, zircon (Zrn), pyrochlore (Pcl), and wöhlerite (Woh). (**c**) Late mineral assemblage in slightly fenitized granite, with aegirine augite (Aug-aeg) replaced by an association of ankerite (Ank), strontianite (Str), barite (Brt), bastnäsite-(Ce) (Bst), and galena (Gn). (**d**) Late replacements in slightly fenitized granite: Ce-rich pyrochlore (Pcl) into biotite (Bt), which is weathered to mixtures of smectite and vermiculite (Sme + Vrm). Zoned ilmenorutile (Rt) is replaced by barite (Brt) and daqingshanite-(Ce) (Daq). Also, note goethite pseudomorphs after pyrite (Gth). (**e**) Late replacements in highly fenitized granite: assemblage of zircon (Zrn), late Ba-rich pyrochlore (Pcl-Ba), rutile (Rt), and quartz (Qz) filling fractures and replacing K-feldspar (Fk) across grain borders. (**f**) Late replacements in highly fenitized granite: rhabdophane-(Ce) (Rpd) and an undetermined Ce-La rich phosphate (PhospLaCe) intergrown with quartz (Qz). Pyrite is replaced by goethite (Gth).

Highly fenitized granites from the innermost areas contain two generations of K-feldspar: the first generation has very fine-grained hematite inclusions whereas a second type does not contain Fe oxides. Late silicification produces interstitial quartz between the feldspar grains, as well as veinlets. Quartz is accompanied by zircon, Ba- and Sr-rich pyrochlore crystals less than 40 μm in diameter (Figure 3e), and tiny fibrous crystals of rhabdophane-(Ce), up to 50 μm in length (Figure 3f).

4.2.3. Magmatic Breccia

Magmatic Breccia with an Alkaline Groundmass

This type of breccia contains carbonatite fragments, thus suggesting the presumable presence of a deeper carbonatite intrusion, despite the fact that it does not crop out at the surface. These breccias tend to contain abundant Nb and REE minerals. Two varieties of breccias with alkaline mesostase were defined: (a) clast-supported alkaline breccias with calciocarbonatite and fenitized granite fragments and (b) matrix-supported breccia with scarce calciocarbonatite grains but a major alkaline groundmass.

In clast-supported alkaline breccias, calciocarbonatite fragments are made up of major coarse calcite, with apatite grains (up to 10 modal %) locally arranged in bands, thus suggesting the existence of magmatic bedding in the original photolith; pyrite (replaced by goethite) and alkaline amphiboles of the richterite-ferrorichterite series can be very abundant, up to about 20 modal %. Euhedral zoned fluornatropyrochlore crystals may be found as inclusions in the calcite or amphibole crystals (Figure 4a). These zoned crystals may reach up to 40 μm in diameter. A secondary association of Sr-, Ba-, REE-carbonates and sulphates replaces the primary assemblages by filling late microfractures and as patches. Strontianite, barite, and rutile are the most abundant phases in this stage, and they are cut or overgrown by radial aggregates of fine-grained (less than 20 μm in length) crystals of synchysite-(Ce), calcioancylite-(Ce), and burbankite (Figure 4b). The compositions of the subsolidus pyrochlore generations depend on the accompanying minerals. Pyrochlore scattered in calcite is replaced by thin rims (up to ten microns) of secondary U- and Th-bearing pyrochlore, whereas pyrochlore included in amphiboles is veined by a late association of Sr-late pyrochlore, quartz, and raphdophane-(Ce).

In matrix-supported alkaline breccia, calciocarbonatite clasts are scarce and surrounded by a reaction rim of fine-grained biotite, K-feldspar, albite, calcite, and trace ilmenite, pyrite, pyrrhotite, REE-carbonates, and pyrochlore. The abundance of alkali-bearing minerals in these rims suggests a strong interaction with the alkaline mesostase. Some of the calciocarbonatite fragments may display up to 50 modal % anhedral fluorite crystals, which may contain inclusions of rounded calcite grains suggesting its simultaneous magmatic crystallization in equilibrium with calcite (Figure 4c). Fluornatropyrochlore, sphalerite, and pyrrhotite are common minerals found as euhedral inclusions in both fluorite and calcite crystals. Late fine-grained calcioancylite-(Ce) and synchysite-(Ce) also occur as anhedral interstitial grains, up to 20 μm in length, scattered across the carbonate.

Two types of alkaline groundmass are observed in the alkaline magmatic breccia:

1. Quartz-syenitic: which tends to be clast-supported and is comprised of reddish K-feldspar and albite with late interstitial quartz and ilmenorutile. Late veinlets contain a new generation of quartz along with hematite, synchysite-(Ce), and barite (Figure 5a, Table 2).

2. Foidolitic: which tends to be groundmass-supported, and feldspathoids (nepheline and sodalite, more or less replaced by cancrinite) are the most abundant minerals, replacing K-feldspar and albite. In addition, fluorapatite, anhedral biotite, calcite, richterite-ferrorichterite and fluornatropyrochlore occur as minor components. Pyrochlore occurs as euhedral inclusions inside all the above-mentioned minerals, suggesting its early crystallization from the melt. Nepheline appears to be associated with zircon. Cancrinite could have an important metallogenetic role, as it often appears intergrown with fluorite, calcioancylite-(Ce), burbankite, and secondary pyrochlore (Figure 4d). Late sodalite replaces albite and nepheline. A new generation of U- and Ti-rich pyrochlore is associated with sodalite and replaced earlier pyrochlore types. Because of its U content, it presents intense fracturing due to metamictization processes (Figure 4e).

Rare rounded ilmenorutile is also overgrown by Mn-rich ilmenite, secondary fine-grained Na-rich-calciopyrochlore, pyrrhotite, and galena (Figure 5b, Table 2).
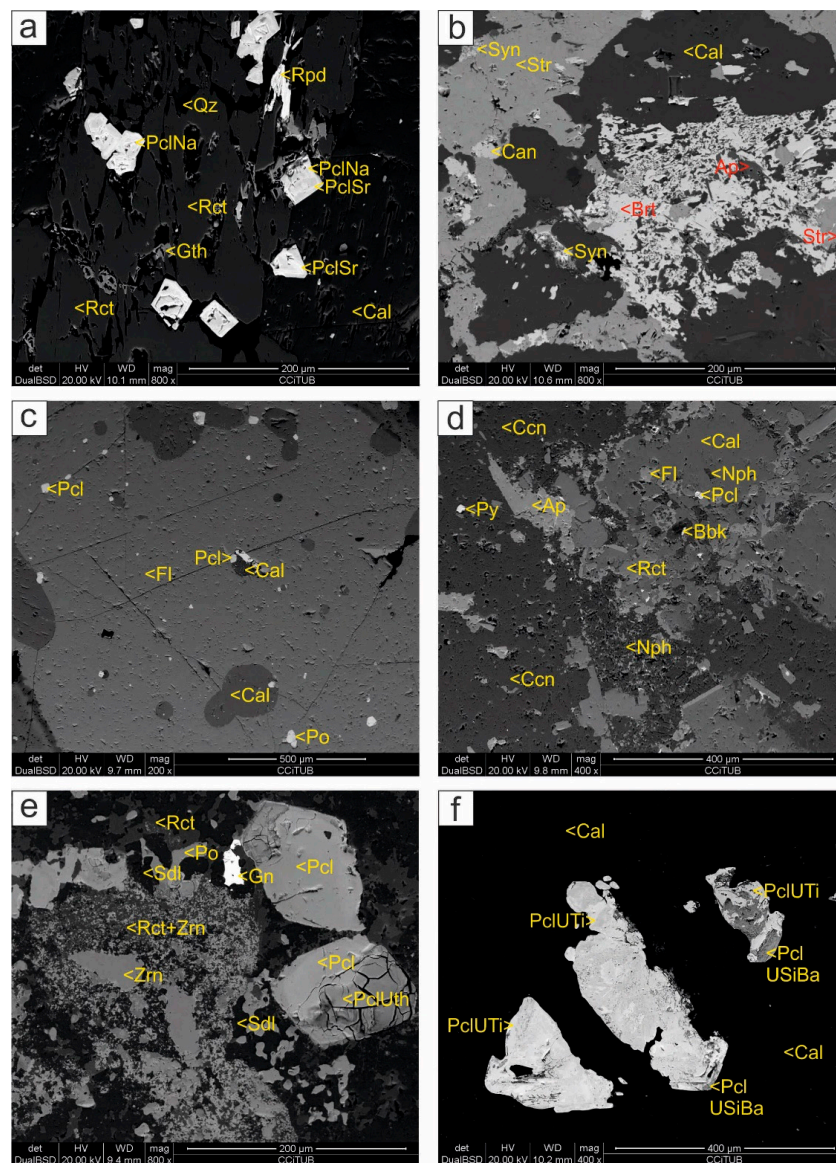
Figure 4. Nb and REE minerals in the Monte Verde breccias; SEM images, BSE mode. (**a**) Detail of a calciocarbonatite xenolith. Fluornatropyrochlore euhedral inclusions in both calcite (Cal) and richterite (Rct). During a hydrothermal event, quartz (Qz) precipitated along grain boundaries of primary minerals, along with rhabdophane-(Ce) (Rbd); primary pyrochlore was replaced by Sr-rich pyrochlore. Note also the goethite produced by weathering of carbonates (Gth). (**b**) Detail of a calciocarbonatite xenolith. Apatite (Ap) and calcite (Cal) replaced by barite (Brt), strontianite (Str), calcioancylite-(Ce) (Can), and synchysite-(Ce) (Syn). (**c**) Detail of a calciocarbonatite xenolith. Co-crystallization in equilibria of fluorite (Fl) with calcite (Cal), fluornatropyrochlore (Pcl), and pyrrhotite (Po). (**d**) Detail of a foidolitic mesostase replacing a carbonatite xenolith. The xenolith has calcite (Cal), fluorapatite (Ap), fluorite (Fl), and fluornatropyrochlore (Pcl). It is surrounded by a reaction rim of richterite (Rct). The ensemble is replaced first by nepheline and then by cancrinite, along with pyrite (Py), and burbankite (Bbk). (**e**) Richterite crystals (Rct), replaced by zircon (Zrn), sodalite (Sdl), pyrrhotite (Po), and galena (Gn). Primary pyrochlore is overgrown by U-Th generation (PclUTh). (**f**) U and Ti-rich pyrochlore (PclUTi) pseudomorphized by later Si-, U-, and Ba-generation (PclUSiBa).
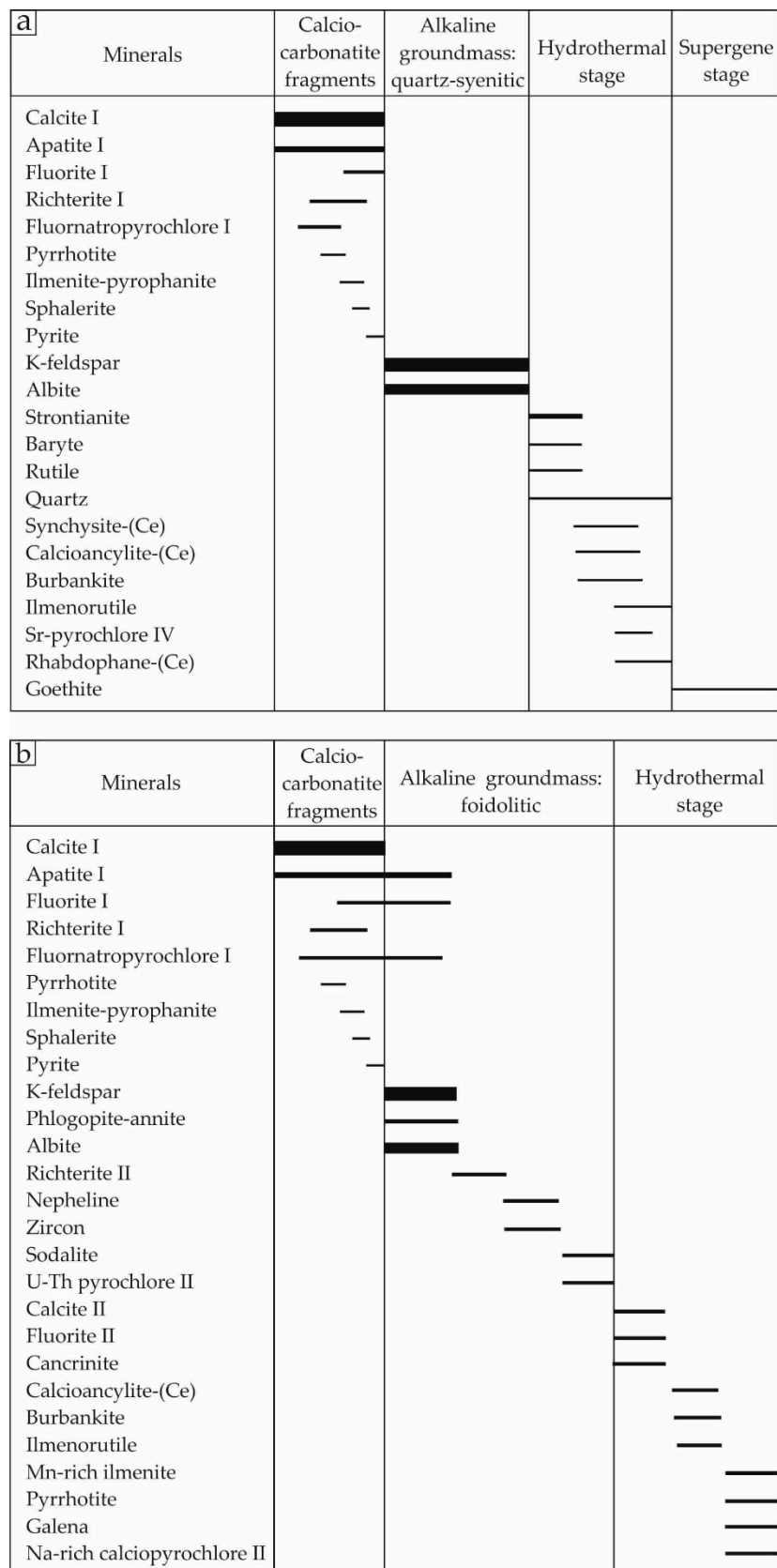
Figure 5. Crystallization sequence of carbonatite breccia; (**a**) carbonatite fragments surrounded by quartz-syenite alkaline groundmass; (**b**) carbonatite fragments surrounded by foidolite alkaline groundmass.

Breccia with Carbonatite Groundmass

Breccia with major calciocarbonatite groundmass contain angular fragments of fenitized granites, although these are partly assimilated by the carbonatite matrix (Figure 6, Table 2). Idiomorphic millimetric calcite is the major phase of the groundmass, reaching up to 80 modal%, with minor aegirine augite. In addition, scarcer fluorapatite displays Sr- and Si-rich rims and may contain fine-grained calcite locally, as well as U-Ti-rich pyrochlore inclusions. U-Ti-pyrochlore also grows as hipidiomorphic crystals of millimetric size among calcite. They are replaced by patches of a late Ba- and Si-rich, U-poor pyrochlore generation (Figure 4f). Scarce burbankite of very fine grain size replaces calcite following the cleavages.

Minerals	K-fenitization	Na-fenitization	Calcio-carbonatite groundmass	Hydrothermal stage	Supergene stage
K-Feldspar	▬▬				
Phlogopite-annite	▬				
Albite		▬▬			
Richterite		—			
Aegirine augite I		—			
Nepheline		—			
Sodalite		—			
Pyrite		—			
Calcite I			▬▬		
Apatite			▬▬		
Aegirine-augite II			—		
U-,Ti-rich pyrochlore III			—		
Mn-rich ankerite				▬▬	
Rutile				▬▬	
Strontianite				—	
Calcioancylite-(Ce)				—	
Burbankite				—	
Barite				—	
Galena				—	
Th-rich bastnäsite-(Ce)				—	
Th-,Ce-rich pyrochlore V				—	
Daqingshanite-(Ce)				—	
Calcite II				—	
Vermiculite				—	
Smectite				—	
Quartz I				▬▬	
Zircon				—	
Ba-,Sr-rich pyrochlore VI				—	
Rhabdophane-(Ce)				—	
Goethite					▬▬
Hematite					▬▬

Figure 6. Sequence of crystallization of carbonatite breccia; (**a**) fenitized granite fragments surrounded by calciocarbonatite groundmass.

4.2.4. Alkaline Dykes

Several swarms of alkaline dykes crosscut all the central intrusive rocks (carbonatites, alkaline breccias, and fenitized granites). According to their composition, four main types of dykes can be distinguished: sodalite-feldspar bearing trachytes, tinguaites, latites, and nepheline trachytes. The latter contain remarkable agpaitic mineral associations enriched in HFSE and REE.

Nepheline trachyte dykes present a clear porphyritic texture defined by major millimetric sanidine and nepheline-kalsilite phenocrysts with lesser aegirine augite, titanite, and ulvöspinel with ilmenite-pyrophanite inclusions. Locally, titanite may contain Nb-rich bands and aegirine augite, pyrite,

and trace rhabdophane-(Ce) inclusions. The alkaline groundmass has major sanidine (0.1–0.5 mm in diameter) intergrown with nepheline and lesser aegirine augite. Secondary sodalite is associated with ulvöspinel and very scarce pyrochlore grains.

In some places, nepheline trachyte dykes show accessory poikilitic crystals of the rosenbuschite and mosandrite-(Ce) group partly replaced by rinkite-(Ce) (Figure 7a). Cancrinite-sodalite late association replaces primary phenocrysts. Together with cancrinite alterations, perovskite crystals among clinopyroxene and titanite may be replaced by loparite-(Ce) veinlets (less than 5 μm in width) and Nb-rich titanite (Figure 7b). In turn, secondary albite pseudomorphizes late feldspathoids.
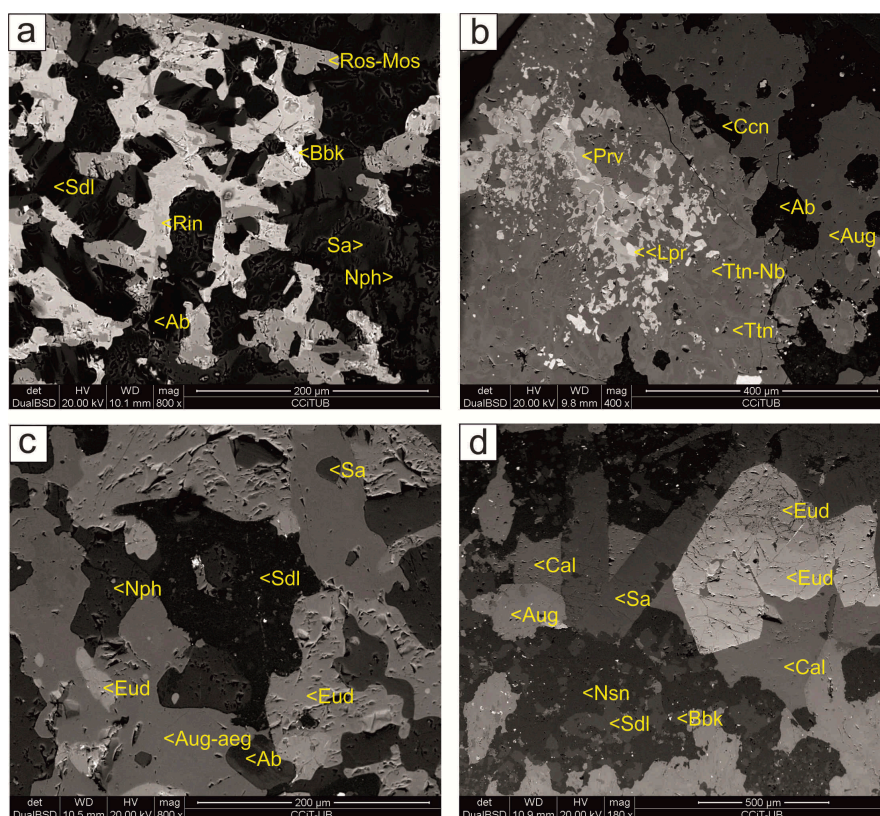
Figure 7. Nb and REE phases in the Monte Verde alkaline dykes. SEM images, BSE mode. (**a**) Rosenbuschite-mosandrite (Ros-Mos) poikilitic crystals replaced by rinkite (Rin) overgrowing sodalite (Sdl), albite (Al), and sanidine (Sa) of the mesostase—replaced by albite (Ab) and burbankite (Bbk). (**b**) Perovskite (Prv) and titanite (Ttn) replaced by loparite (Lpr) and niobian titanite (Ttn-Nb), respectively, with cancrinite (Ccn) and albite (Ab). (**c**) First generation of poikilitic eudialyte (Eud) intergrown with aegirine augite (Aug-aeg), albite (Al), sanidine (Sa), and nepheline (Nph)—replaced by sodalite (Sdl). (**d**) Eudialyte (Eud), aegirine augite (Aug-aeg), sanidine (Sa) replaced by calcite (Cal) associated with sodalite (Sdl), burbankite (Bbk), and nosean (Nsn). Note a late generation of secondary eudialyte overgrowing the former.

Although scarce, Na-K-Ca-Ti-Zr minerals of the eudialyte group are recognized in augite-rich nepheline trachyte dykes. An early eudialyte generation develops poikilitic crystals, up to 1 mm in diameter, intergrown with aegirine augite and nepheline (Figure 7c) associated with late sodalite and replaced by Nb-rich wöhlerite. A second generation of eudialyte replaces the above crystals or occurs in veinlets filled with late calcite and rare burbankite. Secondary eudialyte may form euhedral zoned crystals reaching up to 1 mm in diameter and have strong Mn and Nb enrichments (Figure 7d).

Late generations of albite and calcite have special interest as they are often associated with REE minerals, filling late veins or interstices between nepheline, sanidine, aegirine augite, titanite, and cancrinite-sodalite. Fine carbocernaite and britholite-(Ce) (less than 20 μm) grow with albite.

Locally, late calcite precipitates with ancylite-(Ce) and calcioancylite-(Ce) and may overgrow rosenbuschite-mosandrite together with very fine burbankite aggregates. In addition, tiny veins of albite and acicular synchysite-(Ce) surround them.

4.3. Mineral Chemistry

The mineral composition of the most significant Nb- and REE- phases has been studied—namely, the members of the pyrochlore, perovskite, rinkite, wöhlerite, and eudialyte groups. Results are shown at Supplementary material. Unfortunately, due to the fine-grained size of some of the REE carbonates, it was not possible to obtain good results.

4.3.1. Pyrochlore

Primary (Type I)

The earliest pyrochlore is restricted to the carbonatite breccia unit, the calciocarbonatite fragments, and the feldspathoid-bearing mesostase of foidolite breccias. This pyrochlore commonly displays a homogenous composition. The B-site is mainly occupied by Nb, although Ta and Ti contents can be significant in pyrochlore from the foidolitic mesostase in the breccias, where low Zr, Fe, and Si enrichments have also been recorded (less than 0.05 a.p.f.u.). The A-position mainly contains Na and Ca, ranging from 0.64 to 1 and 0.86 to 1 a.p.f.u., respectively. Na proportion is higher in alkaline groundmass than in carbonatite fragments. Sr, Ce, and Th are very low, whereas U was not detected (Figure 8).

Type I pyrochlore in the fluorite-bearing carbonatite xenoliths shows the lowest REE and HFSE contents. Regarding the Y-site, F is the only anion occupying this position. Type I pyrochlore should be classified as fluornatropyrochlore to fluorcalciopyrochlore according to the criteria of Atencio et al. [42].
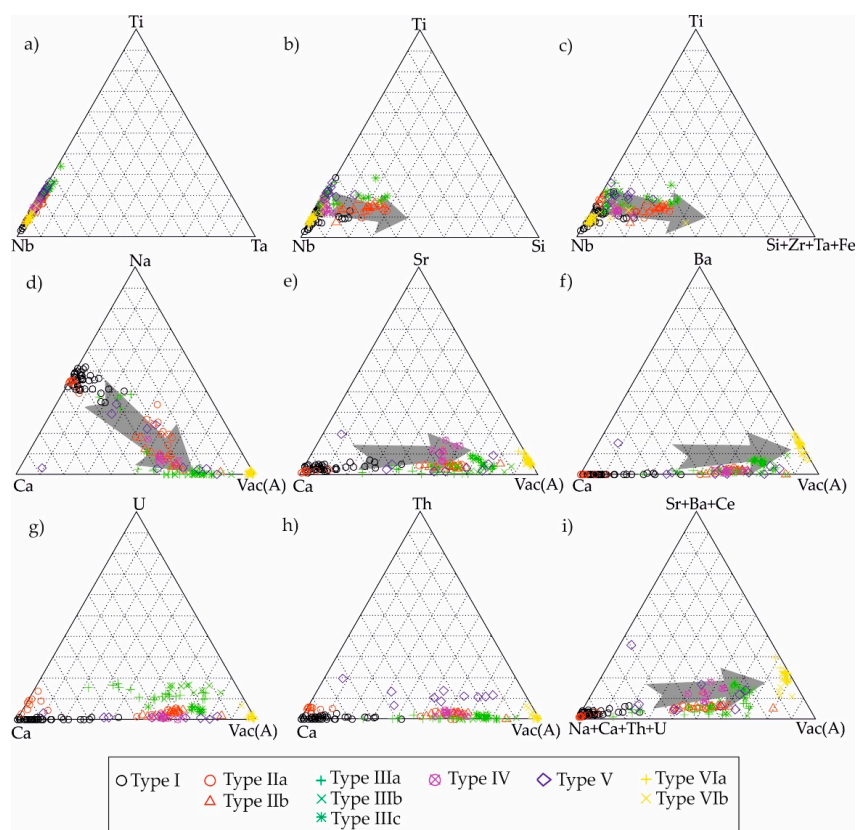
Figure 8. Chemical composition of pyrochlore generations of Monte Verde. Ternary diagrams from (**a**–**c**) correspond to B-site changes, whereas (**d**–**i**) represent the A-site. Grey arrows indicate evolution trends from primary generation to secondary [30,43].

Secondary Pyrochlore (II, III, IV, V, VI Types)

Pyrochlore II occurs in the alkaline matrix of breccia. According to the composition of primary pyrochlore, two subtypes can be recognized. IIa subtype grows within the nepheline-sodalite groundmass and contains remarkable UO_2 and ThO_2 contents, up to 4.08 and 10.54 wt.%, respectively. These elements substitute Na and Ca in the A-site of the pyrochlore structure. SrO and BaO contents are nearly 2.5 wt.%, whereas Ce_2O_3, the dominant LREE, is less than 1 wt.%. The B-site is mostly occupied by Nb, whereas in the Y-site, F is lower than in the earlier fluornatropyrochlore. The second subtype (IIb) occurs in the alkaline groundmass associated with richterite, as fine rims overgrowing zoned primary pyrochlores. It displays a similar composition to the IIa subtype; however, it does not contain Na and UO_2 contents are higher (up to 6.13 wt.%). In both subtypes, Ca is the major cation in A; therefore, they could be classified as hydroxycalciopyrochlore [42].

Pyrochlore III only occurs in the carbonatite mesostase of the breccia. There are significant UO_2 contents in the A-site, major Nb in the B-site, but no F in the Y position have been recorded. Three compositional varieties are identified based on A-site occupancy. The first one has high UO_2 contents (12.39–16.92 wt.%) with high Ce_2O_3 and major vacancies but no Na and low Ca contents. However, the highest UO_2 contents have been recorded into the second subtype, up to 23.07 wt.%, which also includes high BaO amounts and vacancies. Finally, the third subtype is relatively depleted in UO_2 (only up to 7.60 wt.%), with low ThO_2, whereas vacancies are dominant in the A-site.

Pyrochlore IV is located in the carbonatite xenoliths of the breccia, with syenitic mesostase overgrowing or replacing fluornatropyrochlore in association with late quartz and REE minerals. This'secondary pyrochlore has the highest SrO contents, up to 0.29 wt.% although Ca is still the major cation at the A-site and vacancies are predominant. F may reach 4.22 wt.%.

Pyrochlore V mostly occurs in the fenitized granites, associated with secondary biotite, ankerite, ilmenorutile, barite, and rhabdophane-(Ce). Characteristic ThO_2 and Ce_2O_3 enrichments (5.77–14.40 wt.% and 2.55–4.67 wt.%) have been recorded.

The latest type VI pyrochlore concentrates in highly fenitized granites and is intergrown with zircon crystals. Two subtypes were recognized: the first one contains high Ba and Sr at the A-site (up to 0.35 and 0.17 a.p.f.u.) and vacancies, but no Na and Ca. On the other hand, a second subtype crosscuts subtype I and has remarkable ThO_2 and UO_2 enrichments, up to 8.24 and 8.25 wt.%, respectively. Nb is predominant at the B site, whereas the Y-site is fully occupied by OH (Figure 8).

Therefore, III, IV, V, and VI generations can be defined as kenopyrochlore according to Atencio [42], as vacancies are predominant at the A-site.

4.3.2. Perovskite-Loparite-(Ce)

Perovskite occurs in nepheline trachyte dykes associated with late cancrinite alteration, where it is overgrown by loparite-(Ce), Nb, and REE- rich titanite. Perovskite shows significant contents of Ce and La but also Na (up to 0.09, 0.08, and 0.22 a.p.f.u., respectively). However, Nb and Sr contents (corresponding to lueshite and tausonite components) are not significant and may reach up to 0.02 and 0.09 a.p.f.u.

Loparite-(Ce) contains about 0.40 a.p.f.u. of Na and significant Ce, La, and Nd enrichments reaching up to 0.16, 0.12, and 0.02 a.p.f.u., respectively (Figure 9).

Therefore, the evolution trend observed from perovskite to loparite-(Ce) describes Na, REE, Nb, and Th enrichments, as has also been reported in the alkaline complexes of the Kola Peninsula [44,45].
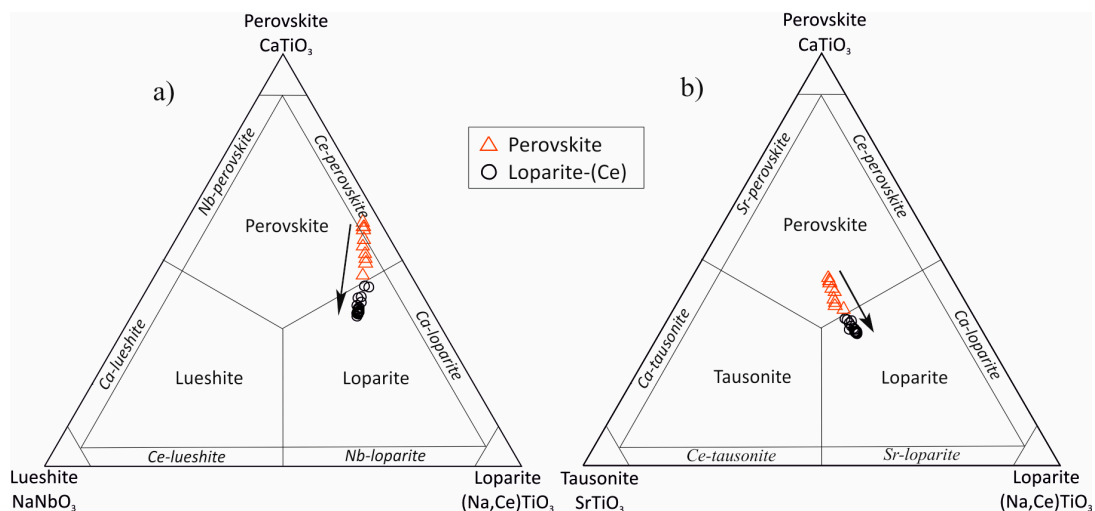
Figure 9. Chemical composition of the perovskite mineral group. (**a**) Ternary diagram $NaNbO_3$-$CaTiO_3$-$(Na,Ce)TiO_3$; (**b**) Ternary diagram $SrTiO_3$-$CaTiO_3$-$(Na,Ce)TiO_3$. Classification diagrams of the perovskite group according to Mitchell [44]. Arrows indicate evolution trends from early perovskite to secondary loparite-(Ce).

4.3.3. Eudialyte

Two types of eudialyte have been distinguished in the nepheline trachyte dykes cutting the central intrusion. The first eudialyte type, of magmatic origin, is intergrown with early nepheline and aegirine augite. High CaO and SrO (up to 15.5 and 2.68 wt.%) and low MnO contents ranging from 2.30 to 2.51 wt.% were recorded (Figure 10). The Z-site is fully occupied by Zr, whereas Nb_2O_5 can reach up to 2.70 wt.%. However, significant amounts of Cl (1.48–1.95 a.p.f.u.) can enter the X-position.

Secondary eudialyte occurs, filling late veins cutting nepheline dykes. It displays concentric zoning, with a core of similar composition to that of eudialyte I but surrounded by Mn- and Nb- richer rims (Figure 10). In addition, rims have high Ce and La contents (1.55 and 1.61 wt.% Ce_2O_3 and La_2O_3, respectively) replacing Na. The X-site of the rims is poor in Cl in comparison to the cores.

4.3.4. Na-Zr-Ti Sorosilicates

Minerals of this group have complex general formulas with high HFSE and REE as well as Mn, Fe, Na, and Ca [46–48], and include the wöhlerite and rinkite groups.

Wöhlerite ($Na_2Ca_4(Zr,Nb)_2(Si_2O_7)_2(O,OH,F)_2$) replaces an early eudialyte generation often concentrating higher Zr than Nb, which is lower than 0.87 a.p.f.u., a low value if it is compared to other alkaline complexes [49]. Ta, REE, Y and halogen contents are negligible.

Rinkite group minerals occur in nepheline trachyte dykes and melteigite rocks as accessory phases.

- Rosenbuschite [$Na_6Ca_6Zr_3Ti(Si_2O_7)_4$] is a characteristic phase of alkaline conditions reflecting low agpaicity as its alkalinity is close to 25% [50,51]. Zr content (1.68–1.80 a.p.f.u.) is higher than that of Nb (0.96–1.04 a.p.f.u.), and Ti (0.41–0.47 a.p.f.u). In addition, Mn and Fe are also remarkable (up to 0.7 and 0.3 a.p.f.u., respectively).
- Mosandrite-(Ce) [$(Ca_3REE)(H_2O)_2Ca_{0.5}\square_{0.5})(Ti(Si_2O_7)(OH)(H_2O)_2$] is an alkaline sorosilicate indicative of almost miaskitic conditions [52]. Ti is the main cation of high charge cations (up to 2.1 a.p.f.u.) with lesser Zr and Nb. In addition, LREE concentrations are high, especially Ce content (up to 0.91 a.p.f.u.); Y and F contents are extremely low.
- Rinkite-(Ce) [$(Ca_3,REE)_4Na(Na,Ca)_2(Ti,Zr,Nb)(Si_2O_7)_2(O,F)_2(H_2O)_2$] usually replaces mosandrite-(Ce) and may suggest an increase of the agpaicity of the rock. Ce is the main LREE (up to 0.46 a.p.f.u.), Ti (0.81–0.96 a.p.f.u) is dominant over Nb and Zr, and F is below detection limit, as in rosenbuschite and mosandrite-(Ce).
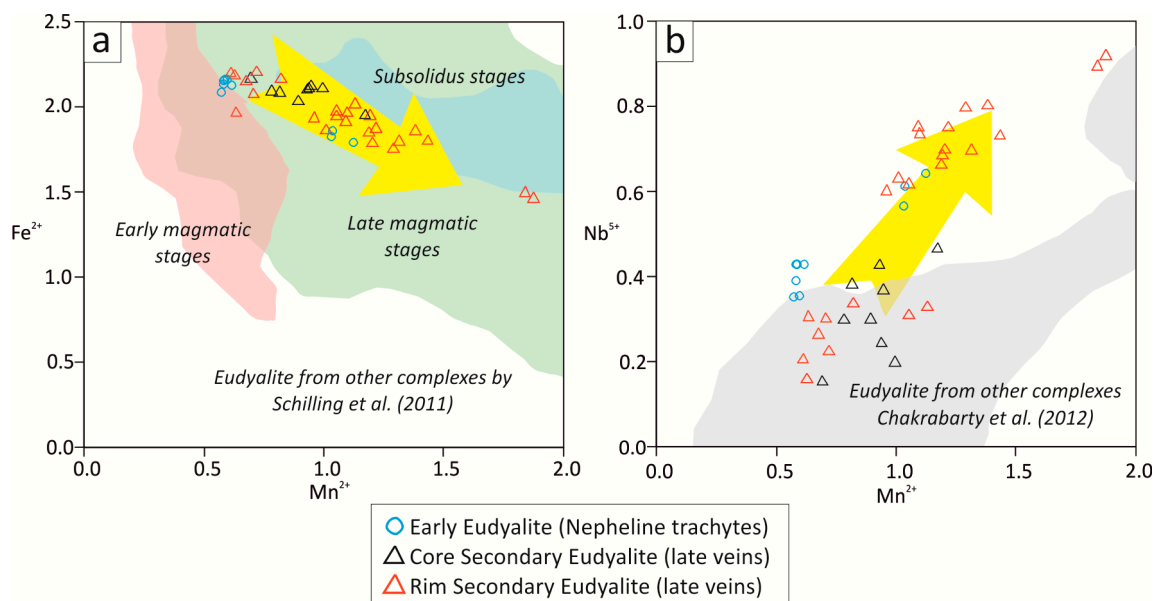
Figure 10. Variation of chemical composition of eudialyte from Monte Verde. (**a**) Mn^{2+} vs. Fe^{2+} diagram; (**b**) Mn^{2+} vs. Nb^{5+} diagram. Eudialyte from Monte Verde is compared to eudialyte from the Illimaussaq (Greenland), Tamazeght (Morocco), and Mount-Saint-Hilaire (Canada) alkaline complexes [53,54]. Yellow arrows indicate the evolution trend of Monte Verde eudialyte.

4.3.5. REE Carbonate Group

Some REE carbonates were found in nepheline trachyte crosscutting both plutonic alkaline rocks and fenitized granites but also in calciocarbonatite fragments of clast-supported breccia of alkaline groundmass. Commonly, they are related to the late stages of the complex formation.

- Monte Verde burbankite $[(Na,Ca)_3(Sr,Ba,Ca,REE)_3(CO_3)_5]$ presents compositional variations, but Na is mostly higher than Ca. In nepheline trachyte dykes, Ce and La are the most abundant LREE (0.21–0.66 and 0.22–0.43 a.p.f.u., respectively). In addition, Ba and Sr may enter the B site reaching high proportions, locally higher than those of LREE. However, in calciocarbonatite xenoliths, burbankite is a trace phase with lower REE and Ba but higher Sr.

- Carbocernaite $[(Ca,Na)(Sr,Ce,Ba)(CO_3)_2]$ is a secondary phase, usually replacing burbankite in nepheline trachyte dykes. Ca contents are higher than Na, and Sr may also be high (up to 0.86 a.p.f.u.). Minor Ba and REE have also been recorded. Ce and La only reach up to 0.16 and 0.12 a.p.f.u., respectively.

- Ancylite-(Ce)-calcioancylite-(Ce) $[(Ca,Sr)_{2-x}REE_x(CO_3)_2(OH)_x(2-x)H_2O]$ correspond to the most abundant REE carbonates of the Monte Verde complex. They often replace earlier REE carbonates generally associated with strontianite and barite. In the nepheline trachyte dykes, ancylite-(Ce) intergrows late calcite and albite, although it can also replace Na-Zr silicates along with titanite and ilmenorutile. Ce contents are about 0.74 a.p.f.u., whereas La and Nd are lower. On the other hand, in calciocarbonatite xenoliths, ancylite-(Ce) exhibits a similar composition but higher ThO_2 contents, which may reach up to 4.79 wt.%.

- Synchysite-(Ce) $[Ca_3(LREE)_2(CO_3)(F,OH)_3]$ forms acicular aggregates overgrowing strontianite, barite, and galena. The previous association replaces the alkaline groundmass of nepheline trachyte dykes. High Ce, La, Nd, and Pr are dominant, with Ce and La as the most important cations reaching up to 1.69 and 0.95 a.p.f.u., respectively. As indicated in the ancylite crystals, ThO_2 may reach up to 3.24 wt.%. The X-site is fully occupied by OH; therefore, synchysite must correspond to a theoretical hydroxylsynchysite-(Ce), although this phase has not been characterized yet.

- Extremely rare REE minerals were identified replacing nepheline in trachyte dykes. Remondite $[Na_3(REE)_3(CO_3)_5]$ is associated with late calcite, both phases filling fine veins. LREE show

high contents, but no HREE have been detected. In addition, a similar phase to kukharenkoite-(Ce) [Ba_4 $(LREE)_2(CO_3)_6F_2$] is associated with hydroxylsynchysite-(Ce), strontianite, and barite, and presents higher Ba contents and Ce as the dominant LREE cation (up to 1.34 a.p.f.u).

4.3.6. REE Silicates and Phosphates

- Britholite-(Ce) [Ca,REE)$_{10}$(Si,PO$_4$)$_6$(OH,F)$_2$] occurs in nepheline trachyte dykes associated with late albite overgrowing nepheline-, sanidine-rich groundmass. Britholite presents up to 5.07 a.p.f.u. Si, whereas Ce and La are the most common LREE cations (up to 2.19 and 1.64 a.p.f.u, respectively). F contents are low (0.2–0.3 a.p.f.u.), which is also the case of Na-Zr-Ti sorosilicates and REE carbonates of Monte Verde.
- Rhabdophane-(Ce) and raphdophane-(La) [(REE,Ca,Th)(PO$_4$)·H_2O] are found in association with quartz veins replacing fenitized granites. They present Ce and La enrichments (up to 0.62 and 0.50 a.p.f.u., respectively) with lesser Nd—which is slightly higher in rhabdophane-(La). Th and HREE are negligible.

5. Discussion

5.1. Evolution of the Monte Verde Complex

Although the amount of geological data is relatively restricted because of the limited size of the outcrops, textural patterns can help to reconstruct the formation history of the complex.

Breccias with carbonatite matrix have fragments of carbonatites and fenitized granites, but the alkaline breccias include fragments of carbonatites. In addition, alkaline dykes crosscut all the existing units. Therefore, the intrusion of alkaline magmas seems to have occurred after the crystallization of the main carbonatite bodies.

The association of carbonatites and alkaline rocks is a well-known fact and has also been documented in the currently active natrocarbonatite volcano at Oldoinyo Lengai in Tanzania. In this case, the existence of magma mingling between a carbonatitic and an undersaturated alkaline magma is assumed [55]. In addition, very recent studies about Italian carbonatite alkaline complexes display an immiscible separation of silicate and carbonatite liquids [56,57].

5.2. Pyrochlore Evolution in Monte Verde

Pyrochlore is a ubiquitous mineral in carbonatites worldwide and can be formed in different generations, which can be used to interpret the sequence of processes during carbonatite crystallization, as established in the Tchivira model [25].

Primary pyrochlore from Monte Verde formed early in the carbonatite crystallization sequence. Its Y site is fully occupied by F, similar to the magmatic pyrochlore of the Tchivira complex [25], owing to the high F activity in the magma chamber. This interpretation is also compatible with the abundant coeval crystallization of this pyrochlore with fluorite and magmatic calcite, as observed in some carbonatite fragments in the carbonatitic magmatic breccia. By contrast, the Bonga carbonatite breccias do not contain F-bearing pyrochlore [30]. This difference could record a different behaviour of F during explosive processes, or a different F content in the primitive magma. The absence of fluorite in Bonga is more suggestive of lower F contents in the Bonga primitive carbonatitic magma by comparison with the Tchivira or Monte Verde carbonatitic magmas. In this sense, it is interesting to take into account that undersaturated alkaline rocks seem to be absent in Bonga, while mixtures with lamprophyric magmas are present [30]. Finally, the A-site contains mostly Na and Ca in similar proportions, as is the case of Tchivira and Bonga, thus reflecting a high Na activity during the early stages of crystallization of the carbonatite magma.

Five secondary pyrochlore types were identified, replacing and overgrowing magmatic pyrochlore. Na and Ca commonly decrease in these pyrochlores, and thus vacancies, Sr, Ba, U, Th, and REE increase to balance charges. This evolution trend observed in all Angolan carbonatites [25–31,33]. Na decrease

can be related to the decrease of Na activity in the magma, which can be associated with the loss of alkalis during fenitization processes [29]. This deficit of alkaline cations in the A position allows for the incorporation of REE, HFSE, and LILE. The enrichment in these elements can be the result of their fractionation in residual fluids. However, LILEs and REE can also be released from the structures of primary carbonates during replacement of primary calcite—which can accommodate these elements at high temperatures [58]. However, as reported by [25,26], Ba and Sr may also (or at least partly) come from the feldspars of the original host granites, carried by the fluids involved in the aforementioned fenitization processes. In any case, these hydrothermal or carbothermal fluids should be enriched in HFSE, LILE, and REE. Therefore, the successive generations of pyrochlore became enriched in these elements. Hence, type II and III record high UO_2 contents, positively correlated to significant Ta_2O_5 enrichment, although Ta is lower than in other carbonatite complexes, such as U-Ta rich pyrochlore in the Sokli complex [59] or in other Angolan carbonatites [25,26,33].

Type II pyrochlore in alkaline rocks from Monte Verde also records a slight Zr and Si enrichment, as it grew into an environment that is mostly made up of primary and secondary silicates including zircon.

Fenitized granites can concentrate pyrochlore V, which shows the highest Th enrichments. In addition, type VI pyrochlore with high Ba and Sr contents is associated with feldspar in highly fenitized areas, thus suggesting (again) that at least part of the cations in pyrochlore from fenites (and perhaps in carbonatites) could originate from the host rock.

5.3. Metallogenetic Potential of the Monte Verde Carbonatites

The greenfield exploration campaign carried out in Monte Verde found only small carbonatite outcrops (Figure 1), in most of the cases poorly mineralized with respect to pyrochlore. However, any discussion on the metallogenetic potential of Monte Verde complex must calculate its potential three-dimensional geometry. The carbonatite occurrences of the Monte Verde complex are restricted to carbonatite-bearing alkaline breccia bodies of decametric size hosted in fenitized granites. However, some of these small outcrops of carbonatite breccias occur up to 2 km away from the central alkaline plug. The distribution in concentric rims of these magmatic breccia outcrops suggests that the structure of Monte Verde could correspond to the inner part of a collapsed caldera, and the breccias could represent channels (ring-faults) of extrusion controlled by subvolcanic explosive processes. A similar mechanism was proposed for Alnö [60] to explain the existence of carbonatite ring dykes in Sweden. Hence, by assuming that the structure could correspond to a partially eroded caldera structure, the area with carbonatite potential should be expanded, and the potential for larger intrusions at depth would still persist. In fact, colluvial materials cover large areas around the core of the complex, and therefore, more distal hidden carbonatite rings could also be present beneath these colluvial sediments. Some of these dykes could be mineralized, as occurs at the nearby Bonga complex, where phoscorites and some but not all of the carbonatite ring dykes were found to be valuable metallogenetic prospects (only those enriched in pyrochlore-magnetite-apatite) [60]. Similar enriched ring dykes were described, for instance, in the Sarfartôq carbonatite complex in Greenland [61]. Therefore, a geophysical survey exploration could help to determine the possible existence of mineralized carbonatites or phoscorites at depth. In particular, the existence of different types of anomalies could be helpful to delimitate the 3D structure at depth and its economic potential [62,63]. These include radioactive anomalies—due to the high contents in Th and U in pyrochlore and other minerals, magnetic anomalies—due to the high magnetite content, or gravimetric anomalies—since large volumes of magnetite can create a noticeable density contrast, or time-domain electromagnetic anomalies—when conductive sulphide deposits are present. These methods have been proven to be effective to determine the 3D structure of carbonatites and alkaline intrusions in several places, such as in Mt Weld, Australia [64]; El Morro, Brazil [65]; Elk Creek, USA [66]; Alnö, Sweden [67], Gallinas Mountains in USA [68]; and Beldih in India [69].

Pyrochlore concentrates most HFSE and REE; however, it occurs in extremely low amounts, less than 1 modal % in most of the studied sections, which is lower than the pyrochlore content in carbonatite ring dykes or magnetite-apatite rocks of the Bonga complex [26,29]. Therefore, in addition

to the reduced number of carbonatite outcrops in the area, the observed pyrochlore content is low in most of the cases. Moreover, the HFSE (including U, Th and Ta) and REE are mainly concentrated in secondary pyrochlore generations, which are heterogeneously distributed. In addition, these late pyrochlore generations occur as complex intergrowths, thus presenting an obstacle for the extraction of these elements in the ores.

Monte Verde carbonatites record extremely scarce REE minerals in the outcropping carbonatites, especially if we compare the proportion of these minerals with those found in the Virulundo, Tchivira, or Bonga massifs [5,7–9]. Although some authors propose a magmatic origin for these elements and barite in other carbonatites (e.g., [70]), the textural evidence and the mineral association with quartz suggest a hydrothermal origin for them, as it was also suggested in Tchivira [25]. Other carbonatites worldwide, for instance, Italian carbonatites [56,57]; the Amba Dongar complex, India [71–73]; the occurrences from Sichuan Province, China [74–76]; or the Montviel deposit, Canada [77–80]; may display similar late REE mineral associations. This interpretation poses a problem since it is difficult to deduce how hydrothermal processes distribute REE minerals within carbonatite. However, in the case of Angolan carbonatites, the proximity to intrusive contacts seems to be a key factor [25]. In the case of Monte Verde, the possible existence of a magma chamber at a certain depth, necessary to support the idea of the collapse caldera (see Martí et al.,2008 [81] and references therein), the resulting hydrothermal alterations could be more developed on the flanks (through ring faults) and at the top of the magma chamber.

In addition, concentrations of industrial minerals such as apatite, magnetite, or barite are irrelevant, at least in the documented outcrops. However, the high fluorite contents associated with high pyrochlore contents in some xenoliths can be a strong indication of the occurrence of interesting mineralized bodies at depth, including both fluorite and pyrochlore resources. In Tchivira, the flanks of the carbonatite intrusions are strongly mineralized in fluorite and secondary generations of pyrochlore replacing primary carbonates along with quartz and ankerite. Contrastingly, fluorite and pyrochlore mineralization in the Monte Verde breccias suggests a different type of evolution, with fluorite as a primary magmatic product and associated with typical magmatic pyrochlore.

As carbonatite breccia very rarely crops out at Monte Verde, laterite deposits with high concentrations of heavy minerals (pyrochlore, magnetite, and apatite), such as those developed at the Bonga or Tchivira complexes [25–27], do not occur, at least, in the known outcrops.

In conclusion, although we dismiss any metallogenetic potential of the outcropping carbonatite breccia units, the studied rocks may point out the possible existence of an important mineralized carbonatite body at greater depths. Therefore, a geophysical study of Monte Verde could contribute to gathering valuable information on the extent of these potential resources.

5.4. Metallogenetic Potential of Alkaline Rocks of Monte Verde

Subsaturated alkaline rocks from alkaline massifs set in continental rifts usually show high contents of characteristic Zr-Ti-Na-Ca silicates termed agpaitic minerals [82]. However, alkaline massifs with no agpaitic phases and mainly comprised of zircon, titanite, and ilmenite are defined as miaskitic [83]. The agpaitic association is made up of more than 450 complex minerals [5,84,85] most of them being exclusive to one or two deposits. Rare elements tend to concentrate at the most subsaturated peralkaline agpaitic rocks [5,86]. On the other hand, ultramafic and mafic plutonic rocks do not usually present rare element economic mineralization—although they contain rare element carriers such as perovskite, apatite, and titanite [9].

Agpaitic complexes often contain rare exclusive phases with highly diverse compositions which reflect the degree of evolution of the alkaline magma [85]. The following descriptive terms are proposed for alkaline rocks according to their magmatic HFSE mineralogy: miaskitic, transitional agpaitic, agpaitic, and hyperagpaitic [85,87].

To evaluate the metallogenetic potential of Monte Verde, a study of agpaicity and alkalinity of the main mineral association was carried out. Alkaline dykes and plutonic rocks mainly show low

agpaitic aegirine augite as the major clinopyroxene. Furthermore, the occurrence of Na-Zr-Ti silicates of the seidozerite supergroup (eudialyte, wöhlerite, rosenbuschite, rinkite, and mosandrite) as well as apatite, titanite, zircon and britholite-(Ce) suggest a low agpaitic association.

Eudialyte is a strategic mineral as it concentrates high Nb, Y, and REE. Eudialyte occurs at Monte Verde as a scarce phase, only found in nepheline trachyte dykes. In addition, andradite-bearing nepheline syenite contains pseudomorphic eudialite that is completely replaced by a secondary association of zircon, wöhlerite, pyrochlore, calcite, and albite. Eudialyte decomposition is described at the kakortokite series of the Illimaussaq complex and resulted in the formation of catapleiite and two phases (A1 and A2) where most of the REE are concentrated [88]. Eudialyte generally exhibits a Fe/Mn > 1 ratio, although the late generation is richer in Mn and REE than the magmatic one—a trend observed in hydrothermal eudialyte from other alkaline complexes worldwide [52,89,90]. However, REE_2O_3 contents measured at Monte Verde are much lower than those found in other alkaline complexes, such as Pilanesberg, South Africa [91]. No significant REE enrichments have been recorded neither in magmatic nor in hydrothermal eudialyte crystals in this study. Thus, eudialyte occurring at Monte Verde is not of high economic interest. Similarly, the scarcity of Na-Zr-Ti silicates of the seidorezite supergroup led to reject the economic importance of the outcropping rocks when compared to economically interesting complexes [92].

Loparite-Ce is the only alkaline phase with high agpaicity. At Monte Verde, loparite-(Ce) occurs as an extremely rare mineral and has low Na contents but significant amounts of Nb and REE (1.12–7.50 wt.% and 18.50–30.45 wt.% Nb_2O_5 and REE_2O_3, respectively) when compared to alkaline complexes of economic interest [50,86]. In the Lovozero massif, Kola Peninsula, loparite-(Ce) is the main ore that is currently being mined for its extremely high REE_2O_3 and Nb_2O_5 enrichments (up to 8–12 wt.% and 30–35 wt.% respectively) [86]. However, because of the scarcity of loparite-(Ce) at Monte Verde alkaline dykes, its economic potential for HFSE and REE is also low.

The contents of pyrochlore are very low in the alkaline rocks, and therefore, the main potential ores in these rocks are loparite and eudialyte. The potential for Ta, U, and Th is more reduced than in the carbonatites.

The activity of volatile elements (F and Cl) should be taken into account in order to assess the HFSE potential, as Cl is an important REE carrier, even more than F, in igneous rocks [93,94]. As mentioned, although mosandrite, rosenbuschite, and rinkite of Monte Verde contain very low F, eudialyte has significant Cl contents. However, the occurrence of large amounts of fluorite in carbonatite xenoliths in the breccias suggests that F activity was high in some stages of crystallization, at least in the carbonatites.

Moreover, as mentioned above, the outcropping area can be considered as the apical part of the complex, and therefore, the existence of mineralization (although scarce) in the dykes opens the possibility that the mineralization can also be present in their buried plutonic equivalents.

6. Conclusions

The Monte Verde complex presents an association of alkaline rocks and carbonatitic and alkaline magmatic breccias. The magmatic breccias draw circular outcrops around a central alkaline plug, which could be indicative of the existence of a collapse caldera structure of nearly 5 km radius, partly covered by colluvial sediments. Based on field and textural evidence, we conclude that the intrusions of the alkaline breccias and dykes were produced later than that of the carbonatite breccias.

Although the carbonatite breccias are poorly mineralized in pyrochlore, some carbonatite fragments coming from a deeper carbonatitic magma chamber are strongly mineralized in primary magmatic fluorite and pyrochlore, suggesting the presence of well-mineralized bodies at depth.

Despite the fact that outcropping alkaline undersaturated plutonic rocks are poorly mineralized in REE and Nb, the occurrence of some moderate to hyperagpaitic minerals in the dykes, including eudialyte, loparite-(Ce), and minerals of the rinkite, rosenbuschite, and wöhlerite groups, could also be indicative of critical element mineralization in the plutonic equivalents at depth. Moreover, the occurrence of later evolved eudialyte can also be indicative of a certain grade of

mineralizing processes in the magma chamber. All these results encourage the geophysical exploration of the massif.

References

1. Nielsen, T.F.D. The petrology of a melilitolite, melteigite, carbonatite and syenite ring dike system, in the Gardiner complex, East Greenland. *Lithos* **1980**, *13*, 181–197. [CrossRef]

2. Kogarko, L.N.; Kononova, V.A.; Orlova, M.P.; Wooley, A.R. *Alkaline Rocks and Carbonatites of the World*; Chapman and Hall: London, UK, 1995; pp. 1–226.

3. Mariano, A.N. Economic Geology of Rare Earth Minerals. In *Geochemistry and Mineralogy of Rare Earth Elements*; Lipman, B.R., KcKay, G.A., Eds.; Mineralogical Society of America: Chantilly, VA, USA, 1989; Volume 21, pp. 303–337.

4. Steenfelt, A. High-technology metals in alkaline and carbonatitic rocks in Greenland: Recognition and exploration. *J Geochem. Explor.* **1991**, *40*, 263–279. [CrossRef]

5. Sørensen, H. Agpaitic nepheline syenites: A potential source of rare elements. *Appl. Geochem.* **1992**, *7*, 417–427. [CrossRef]

6. Pell, J. Mineral deposits associated with carbonatites and related alkaline igneous rocks. In *Undersaturated Alkaline Rocks: Mineralogy, Petrogenesis and Economic Potential*; Mitchell, R.H., Ed.; Mineralogical Association of Canada: Québec, QC, Canada, 1996; Volume 24, pp. 271–310.

7. Sørensen, H. The Ilímaussaq Alkaline Complex, South Greenland—An Overview of 200 years of research and outlook. Contribution to the mineralogy of Ilímaussaq no. 130. *Medd. Grønland Greenl. Geosci.* **2006**, *45*, 1–70.

8. Woolley, A.R. *Alkaline Rocks and Carbonatites of the World*; Geological Society of London: London, UK, 2001; pp. 1–372.

9. Arzamastsev, A.A.; Bea, F.; Arzamastseva, L.V.; Montero, P. Rare earth elements in rocks and minerals from alkaline plutons of the Kola Peninsula, NW Russia, as indicators of alkaline magma evolution. *Rus. J. Earth Sci.* **2002**, *4*, 187–209. [CrossRef]

10. Arzamastsev, A.A.; Yakovenchuk, V.; Pakhomovsky, Y.; Ivanyuk, G. The Khibina and Lovozero alkaline massifs: Geology and unique mineralization. In *Guidebook 33 IGC Excursion*; IUGS: Oslo, Norway, 2008; Volume 47, p. 58.

11. Arzamastsev, A.A.; Arzamastseva, L.V.; Zhirova, A.M.; Glaznev, V.N. Model of formation of the Khibiny-Lovozero ore bearing volcanic-plutonic complex. *Geol. Ore Depos.* **2013**, *55*, 341–356. [CrossRef]

12. Chakhmouradian, A.R.; Zaitsev, A.N. Rare earth mineralization in igneous rocks: Sources and processes. *Elements* **2012**, *8*, 347–353. [CrossRef]

13. Chakhmouradian, A.R.; Wall, F. Rare earth elements: Minerals, mines, magnets (and more). *Elements* **2012**, *8*, 333–340. [CrossRef]

14. Smith, M.P.; Moore, K.; Kavecsánszki, D.; Finch, A.A.; Kynicky, J.; Wall, F. From mantle to critical zone: A review of large and giant-sized deposits of the rare earth elements. *Geosci. Front.* **2016**, *7*, 315–334. [CrossRef]

15. Goodenough, K.M.; Schilling, J.; Jonsson, E.; Kalvig, P.; Charles, N.; Tuduri, J.; Deady, E.A.; Sadeghi, M.; Schiellerup, H.; Müller, A.; et al. Europe's rare earth element resource potential: An overview of REE metallogenetic provinces and their geodynamic setting. *Ore Geol. Rev.* **2016**, *72*, 838–856. [CrossRef]

16. Dostal, J. Rare earth element deposits of alkaline igneous rocks. *Resources* **2017**, *6*, 34. [CrossRef]

17. Chakhmouradian, A.R.; Mitchell, R.H. Primary, agpaitic and deuteric stages in the evolution of accessory Sr, REE, Ba and Nb-mineralization in nepheline-syenite pegmatites at Pegmatite Peak, Bearpaw Mts, Montana. *Mineral. Petrol.* **1999**, *67*, 85–110. [CrossRef]

18. Markl, G. Stability of Na–Be minerals in late-magmatic fluids of the Ilímaussaq alkaline complex, South Greenland. *Geol. Surv. Den. Greenl.* **2001**, *190*, 145–158.

19. Barton, M.D.; Young, S. Non-pegmatitic deposits of beryllium-Mineralogy, geology, phase equilibria and origin. *Rev. Mineral. Geochem.* **2002**, *50*, 591–691. [CrossRef]

20. Foley, N.K.; Jaskula, B.W.; Piatak, N.M.; Schulte, R.F. *Critical Mineral Resources of the United States-Economic and Environmental Geology and Prospects for Future Supply*; Schulz, K.J., DeYoung, J.H., Jr., Seal, R.R., II, Bradley, D.C., Eds.; U.S. Geological Survey: Reston, VA, USA, 2017; pp. E1–E32.

21. Lyalina, L.M.; Selivanova, E.A.; Zozulya, D.R.; Ivanyuk, G.Y. Beryllium mineralogy of the Kola Peninsula, Russia—a review. *Minerals* **2019**, *9*, 12. [CrossRef]

22. Mitchell, R.H. Carbonatites and carbonatites and carbonatites. *Can. Mineral.* **2005**, *43*, 2049–2068. [CrossRef]

23. Lapido-Loureiro, F.E.V. Carbonatitos de Angola. *Memórias Trab. Inst. Investig. Científica Angola* **1973**, *11*, 1–242.

24. Issa Filho, A.; Dos Santos, A.B.R.M.D.; Riffel, B.F.; Lapido-Loureiro, F.E.V.; McReath, I. Aspects of the geology, petrology and chemistry of some Angolan carbonatites. *J. Geochem Explor.* **1991**, *40*, 205–206. [CrossRef]

25. Bambi, A.J.M.; Costanzo, A.; Gonçalves, A.O.; Melgarejo Draper, J.C. Tracing chemical evolution of primary pyrochlore from plutonic to volcanic carbonatites: The role of F. *Mineral. Mag.* **2012**, *76*, 377–392. [CrossRef]

26. Bambi, A.J.M. Metalogenia de Las Carbonatitas en Dominios Plutónicos, Subvolcánicos y Volcánicos: Tchivira, Bonga y Catanda, Angola. Ph.D. Thesis, Universitat de Barcelona, Barcelona, Spain, November 2015.

27. Zheng, L.; Gu, X.; Zhang, Y. Pyrochlore chemistry from the Bonga carbonatite type Nb deposit, Huila Province, Angola: Implications for magmatic-processes of carbonatite. *Acta Geol. Sin.* **2014**, *2*, 487–488. [CrossRef]

28. Amores, S. Evolución Metalogenética de Complejos Carbonatíticos en Contexto Hipoabisal y Plutónico: Bonga y Monte Verde (Angola). Ph.D. Thesis, Universitat de Barcelona, Barcelona, Spain, September 2017.

29. Amores-Casals, S.; Melgarejo, J.C.; Bambi, A.C.J.M.; Gonçalves, A.O.; Morais, E.; Manuel, J.; Costanzo, A.; Martí Molist, J. Lamprophyre—Carbonatite magma mingling and subsolidus processes as key controls on critical elements enrichment in carbonatites: The Bonga complex (Angola). *Minerals* **2019**, *9*, 601. [CrossRef]

30. Melgarejo, J.C.; Costanzo, A.; Bambi, A.C.J.M.; Gonçalves, A.O.; Neto, B.N. Subsolidus processes as a key factor on the distribution of Nb species in plutonic carbonatites: The Tchivira case, Angola. *Lithos* **2012**, *152*, 187–201. [CrossRef]

31. Torró, L.; Villanova, C.; Castillo, M.; Campeny, M.; Gonçalves, A.O.; Melgarejo, J.C. Niobium and rare earth minerals from the Virulundo carbonatite, Namibe, Angola. *Mineral. Mag.* **2012**, *76*, 393–409. [CrossRef]

32. Castellano, A.; Melgarejo, J.C.; Bambi, A.C.J.M.; Gonçalves, A.O.; Alfonso, P. Nb and REE at the Bailundo carbonatite, Angola. In *Let's Talk Ore Deposits*; Barra, F., Ed.; Universidad Católica del Norte: Antofagasta, Chile, 2011; pp. 675–677.

33. Campeny, M. Caracterización del Vulcanismo Carbonatítico de Catanda. Ph.D. Thesis, Universitat de Barcelona, Barcelona, Spain, November 2015.

34. Alberti, A.; Castorina, F.; Censi, P.; Comin-Chiaramonti, P.; Gomes, C.B. Geochemical characteristics of Cretaceous carbonatites from Angola. *J. Afr. Earth Sci.* **1999**, *29*, 735–759. [CrossRef]

35. Comin-Chiaramonti, P.; Barros Gomes, C.; Cundari, A.; Castorina, F.; Censi, P. A review of carbonatitic magmatism in the Paraná-Angola-Namibia (PAN) system. *Period. Mineral.* **2007**, *76*, 25–78.

36. Pereira, E.; Rodrigues, J.; Reis, B. Synopsis of Lunda geology, NE Angola: Implications for diamond explorations. *Comun. Inst. Geol. Mineiro* **2003**, *90*, 189–212.

37. Robles-Cruz, S.E.; Escayola, M.; Jackson, S.; Galí, S.; Pervov, V.; Watangua, M.; Gonçalves, A.; Melgarejo, J.C. U-Pb SHRIMP geochronology of zircon from the Catoca kimberlite, Angola. Implication for diamond exploration. *Chem. Geol.* **2012**, *310–311*, 137–147. [CrossRef]

38. Castillo-Oliver, M.; Galí, S.; Melgarejo, J.C.; Griffin, W.L.; Belousova, E.; Pearson, N.J.; Watangua, M.; O'Reilly, S.Y. Trace-element geochemistry and U – Pb dating of perovskite in kimberlites of the Lunda Norte Province (NE Angola): Petrogenetic and tectonic implications. *Chem. Geol.* **2016**, *426*, 118–134. [CrossRef]

39. Giuliani, A.; Campeny, M.; Kamenetsky, V.; Alfonso, J.C.; Maas, R.; Melgarejo, J.C.; Kohn, B.P.; Matchan, E.L.; Mangas, J.; Gonçalves, A.O.; et al. Southwestern Africa on the burner: Pleistocene carbonatite volcanism linked to deep mantle upwelling in Angola. *Geology* **2017**, *45*, 971–974. [CrossRef]

40. Morogan, V.; Woolley, A.R. Fenitization at the Alnö carbonatite complex, Sweden; distribution, mineralogy and genesis. *Contrib. Mineral. Petrol.* **1988**, *100*, 169–182. [CrossRef]

41. Le Bas, M.J. Fenites associated with carbonatites. *Can. Mineral.* **2008**, *46*, 915–932. [CrossRef]

42. Atencio, D.; Andrade, M.B.; Christy, A.G.; Gieré, R.; Kartashov, P.M. The pyrochlore supergroup of minerals: Nomenclature. *Can. Mineral.* **2010**, *48*, 673–698. [CrossRef]

43. Lumpkin, G.R.; Ewing, R.C. Geochemical alteration of pyrochlore group minerals: Pyrochlore subgroup. *Am. Mineral.* **1995**, *80*, 732–743. [CrossRef]

44. Chakhmouradian, A.R.; Mitchell, R.H. Compositional variation of perovskite-group minerals from the Khibina complex, Kola peninsula, Russia. *Can. Mineral.* **1998**, *36*, 953–969.

45. Mitchell, R.H.; Welch, M.D.; Chakhmouradian, A.R. Nomenclature of the perovskite supergroup: A hierarchical system of classification based on crystal structure and composition. *Mineral. Mag.* **2017**, *81*, 411–461. [CrossRef]

46. Shibayeva, R.I.; Belov, N.V. Crystal structure of wöhlerite, $Ca_2Na(Zr,Nb)Si_2O_7(O,F)_2$. *Dokl. Akad. Nauk SSSR* **1960**, *146*, 897–900.

47. Bellezza, M.; Merlino, S.; Perchiazzi, N. Chemical and structural study of te Zr, Ti-disilicates in the venanzite from Pian di Celle, Umbria, Italy. *Eur. J. Mineral.* **2004**, *16*, 957–969. [CrossRef]

48. Biagioni, C.; Merlino, S.; Parodi, G.C.; Perchiazzi, N. Crystal chemistry of minerals of the wöhlerite group from the Los archipelago, Guinea. *Can. Mineral.* **2012**, *50*, 593–609. [CrossRef]

49. Mariano, A.N.; Roeder, P.L. Wöhlerite: Chemical composition, cathodolumniscence and environment of crystallization. *Can. Mineral.* **1989**, *27*, 709–720.

50. Vlasov, K.A. Geochemistry and mineralogy of rare elements and genetic types of their deposits. In *Geochemistry of Rare Elements*; Vlasov, K.A., Ed.; Israel Program for Scientific Translations: Jerusalem, Israel, 1966; Volume 1, p. 688.

51. Mitchell, R.H.; Chakhmouradian, A.R. Compositional variation of loparite from the Lovozero alkaline complex, Russia. *Can. Mineral.* **1996**, *34*, 977–990.

52. Christiansen, C.; Johnsen, O.; Makovicky, E. Crystal chemistry of rosenbuschite group. *Can. Mineral.* **2003**, *41*, 1203–1224. [CrossRef]

53. Schilling, J.; Wu, F.Y.; McCammon, C.; Wenzel, T.; Marks, M.A.W.; Pfaff, K.; Jacob, D.E.; Markl, G. The compositional variability of eudialyte group minerals. *Mineral. Mag.* **2011**, *75*, 87–115. [CrossRef]

54. Chakrabarty, A.; Pruseth, K.L.; Sen, A.K. Composition and Petrogenetic significance of the Eudialyte group minerals from Sushina, Purulia, West Bengal. *J. Geol. Soc. India* **2012**, *79*, 449–459. [CrossRef]

55. Dawson, J.B.; Smith, J.V.; Steele, I.M. 1966 ash eruption of the carbonatite volcano Oldoinyo Lengai: Mineralogy of lapilli and mixing of silicate and carbonate magmas. *Mineral. Mag.* **1992**, *56*, 1–16. [CrossRef]

56. Stoppa, F.; Pirajno, F.; Schiazza, M.; Vladykin, N.V. State of art: Italian carbonatites and their potential for critical metal deposits. *Gondwana Res.* **2016**, *37*, 152–171. [CrossRef]

57. Stoppa, F.; Schiazza, M.; Rosatelli, G.; Castorina, F.; Sharygin, V.V.; Ambrosio, F.A.; Vicentini, N. Italian carbonatite system: From Mantle to ore-deposits. *Ore Geol. Rev.* **2019**, *114*, 103041. [CrossRef]

58. Chakhmouradian, A.; Reguir, E.; Couëslan, C.; Yang, P. Calcite and dolomite in intrusive carbonatites. II. Trace-element variations. *Mineral. Petrol.* **2016**, *110*, 361–377. [CrossRef]

59. Lee, M.J.; Lee, J.I.; Garcia, D.; Moutte, J.; Williams, T.; Wall, F.; Kim, Y. Pyrochlore chemistry from the Sokli phoscorite-carbonatite complex, Finland: Implications for the genesis of phoscorite and carbonatite association. *Geochem. J.* **2006**, *40*, 1–13. [CrossRef]

60. Andersson, M.; Malehmir, A.; Troll, V.R.; Dehghannejad, M.; Juhlin, C.; Ask, M. Carbonatite ring-complexes explained by caldera-style volcanism. *Sci. Rep.* **2013**, *3*, 1677. [CrossRef]

61. Secher, K.; Larsen, L.M. Geology and mineralogy of the Sarfartôq carbonatite complex, southern West Greenland. *Lithos* **1980**, *13*, 199–212. [CrossRef]

62. Hoover, D.B. Geophysical model of carbonatites. In *The Geophysical Expression of Selected Mineral Deposit Models*; Hoover, D.B., Heran, W.D., Hill, P.L., Eds.; U.S. Geological Survey: Reston, VA, USA, 1992; pp. 80–84.

63. Gunn, P.J.; Dentith, M.C. Magnetic responses associated with mineral deposits. *AGSO J. Aust. Geol. Geophys.* **1997**, *17*, 145–158.

64. Duncan, R.K.; Willett, G.C. Mount Weld carbonatite. In *Geology of the Mineral Deposits of Australia and Papua New Guinea*; Hughes, E.E., Ed.; Australasian Institute of Mining and Metallurgy: Carlton, Australia, 1990; Volume 14, pp. 591–597.

65. Alva-Valdivia, L.M.; López-Loera, H. A review of iron oxide transformations, rock magnetism and interpretation of magnetic anomalies: El Morro Mine (Brazil), a case study. *Geofís. Int.* **2011**, *50*, 341–362.

66. Drenth, B.J. Geophysical expression of a buried niobium and rare earth element deposit: The Elk Creek carbonatite, Nebraska, USA. *Interpretation* **2014**, *2*, SJ23–SJ33. [CrossRef]

67. Andersson, M.; Malehmir, A. Unravelling the internal architecture of the Alnö alkaline and carbonatite complex (central Sweden) using 3D models of gravity and magnetic data. *Solid Earth Discuss* **2017**, 1–35. [CrossRef]

68. Li, M.; Zhou, X.; Gammons, C.H.; Khalil, M.; Speece, M. Aeromagnetic and spectral expressions of rare earth element depositsin Gallinas Mountains area, Central New Mexico, USA Interpretation. *Explor. Geophys. Assoc. Petr. Geol. Mem.* **2018**, *6*, 1–13.

69. Maurya, A.K.; Dwivedi, A.K.; Mohan, R.; Kumar, A.; Panda, A. Geophysical modeling of heliborne magnetic and TEM data of Beldih alkaline-carbonatite complex, Nort Singhbhum shear zone, India: Implication for uranium-REE exploration. *Explor. Res. At. Miner.* **2019**, *27*, 99–113.

70. Néron, A.; Bédard, L.P.; Gaboury, D. The Saint-Honoré carbonatite REE zone, Québec, Canada: Combined magmatic and hydrothermal processes. *Minerals* **2018**, *8*, 397. [CrossRef]

71. Simonetti, A.; Bell, K.; Viladkar, S.G. Isotopic data from the Amba Dongar Carbonatite Complex, west-central India: Evidence for an enriched mantle source. *Chem. Geol.* **1995**, *122*, 185–198. [CrossRef]

72. Doroshkevich, A.G.; Viladkar, S.G.; Ripp, G.S.; Burtseva, M.V. Hydrothermal REE mineralization in the Amba Dongar carbonatite complex, Gujarat, India. *Can. Mineral.* **2009**, *47*, 1105–1116. [CrossRef]

73. Viladkar, S.; Magna, T.; Rapprich, V.; Hopp, J.; Čejková, B. Nb-V-enriched sövites of the northeastern and eastern part of the Amba Dongar carbonatite ring dike, India. *Geochemistry* **2019**, in press.

74. Liu, Y.; Chakhmouradian, A.R.; Hou, Z.Q.; Song, W.L.; Kynický, J. Development of REE mineralization in the giant Maoniuping deposit (Sichuan, China): Insights from mineralogy, fluid inclusions, and trace-element geochemistry. *Miner. Depos.* **2018**, *54*, 701–718. [CrossRef]

75. Guo, D.X.; Liu, Y. Occurrence and geochemistry of bastnäsite in carbonatite-related REE deposits, Mianning-Dechang REE belt, Sichuan Province, SW China. *Ore Geol. Rev.* **2019**, *107*, 266–282. [CrossRef]

76. Zheng, X.; Liu, Y. Mechanisms of element precipitation in carbonatite-related rare earth element deposits: Evidence from fluid inclusions in the Maoniuping deposit, Sichuan Province, southwestern China. *Ore Geol. Rev.* **2019**, *107*, 218–238. [CrossRef]

77. Nadeau, O.; Cayer, A.; Pelletier, M.; Stevenson, R.; Jébrak, M. The paleoproterozoic Montviel carbonatite-hosted REE-Nb deposit, Abitibi, Canada: Geology, mineralogy, geochemistry and genesis. *Ore Geol. Rev.* **2015**, *67*, 314–335. [CrossRef]

78. Nadeau, O.; Stevenson, R.; Jébrak, M. Evolution of Montviel alkaline–carbonatite complex by coupled fractional crystallization, fluid mixing and metasomatism—Part II: Trace element and Sm-Nd isotope geochemistry of metasomatic rocks: Implication for REE-Nb mineralization. *Ore Geol. Rev.* **2016**, *72*, 1163–1173. [CrossRef]

79. Edahbi, M.; Plante, B.; Benzaazoua, M.; Pelletier, M. Geochemistry of rare earth elements within waste rocks from the Montviel carbonatite deposit, Quebec, Canada. *Environ. Sci. Pollut. Res.* **2018**, *25*, 10997–11010. [CrossRef] [PubMed]

80. Edahbi, M.; Plante, B.; Benzaazoua, M.; Kormos, L.; Pelleter, M. Rare earth elements (La, Ce, Pr, Nd and Sm) from a carbonatite deposit: Mineralogical charcterization and geochical behavior. *Minerals* **2018**, *8*, 55. [CrossRef]

81. Martí, J.; Geyer, A.; Folch, A.; Gottsmann, J. A review on collapse caldera modelling. In *Caldera Volcanism: Analysis, Modelling and Response*; Gottsmann, J., Martí, J., Eds.; Elsevier: Amsterdam, The Netherlands, 2008; pp. 233–283.

82. Kampunzu, A.; Mohr, P. Magmatic evolution and petrogenesis in the East African Rift system. In *Magmatism in Extensional Settings, the Phanerozoic African Plate*; Kampunzu, A.B., Lubala, R.T., Eds.; Springer: Berlin, Germany, 1991; pp. 85–136.

83. Le Maitre, R.W.; Streckeisen, A.; Zanettin, B.; Le Bas, M.J.; Bonin, B.; Bateman, P.; Bellieni, G.; Dudek, A.; Efremova, S.; Keller, J.; et al. Recommendations of the International Union of Geological Sciences Subcommission on the Systematics of Igneous Rocks. In *Igneous Rocks: A Classification and Glossary of Terms*; Le Maitre, R.W., Ed.; University of Tasmania: Hobart, Australia, 2003; p. 250.

84. Dudkin, O.B. Asociaciones minerales agpaíticas. In *Atlas De Asociaciones Minerales En Lámina Delgada*; Melgarejo, J.C., Ed.; Edicions UB: Barcelona, Spain, 1997; pp. 153–160.

85. Marks, M.A.W.; Markl, G. A global review on agpaitic rocks. *Earth Sci. Rev.* **2017**, *173*, 229–258. [CrossRef]

86. Kogarko, L.N.; Williams, C.T.; Woolley, A.R. Chemical evolution and petrogenetic implications of loparite in the layered, agpaitic Lovozero complex, Kola Peninsula, Russia. *Mineral. Petrol.* **2002**, *74*, 1–24.

87. Khomyakov, A.P. *Mineralogy of Hyperagpaitic Alkaline Rocks*; Clarendon Press: Oxford, UK, 1995; p. 223.

88. Karup-Møller, S.; Rose-Hansen, J. New data on eudialyte decomposition minerals from kakortokites and associated pegmatites of the Illimaussaq complex, South Greenland. *Bull. Geol. Soc. Den.* **2013**, *61*, 47–70.

89. Johnsen, O.; Gault, R.A. Chemical variation in eudialyte. *Neues Jahrb. Mineral. Abh.* **1997**, *171*, 215–231.

90. Harris, C.; Cressey, G.; Bell, J.D.; Atkins, F.B.; Beswetherick, S. An occurrence of rare-earth-rich eudialyte from Ascension Island, South Atlantic. *Mineral. Mag.* **1982**, *46*, 421–425. [CrossRef]

91. Olivo, G.R.; Williams-Jones, A.E. REE-rich eudialyte from the Pilanesberg complex, South Africa. *Can. Mineral.* **1999**, *37*, 653–663.

92. Sokolova, E.; Cámara, F. The seidozerite supergroup of TS-block minerals: Nomenclature and classification, with change of the following names: Rinkite to rinkite-(Ce), mosandrite to mosandrite-(Ce), hainite to hainite-(Y) and innelite-1T to innelite-1A. *Mineral. Mag.* **2017**, *81*, 1457–1484. [CrossRef]

93. Migdisov, A.A.; Williams-Jones, A.E. A spectrophotometric study of neodymium (III) complexation in chloride solutions. *Geochim. Cosmochim. Acta* **2002**, *66*, 4311–4323. [CrossRef]

94. Salvi, S.; Williams-Jones, A.E. Alkaline granite-syenite deposits. In *Rare Element Geochemistry and Mineral Deposits*; Linnen, R.L., Samson, I.M., Eds.; Geological Association of Canada: St. John's, NL, Canada, 2015; pp. 315–341.